A MERTK-Targeting Antibody–Drug Conjugate Selectively Depletes M2 Tumor-Associated Macrophages and MERTK-Expressing Cancer Cells

Shugaku Takeda[1], Subhasree Sridhar[1], Daniel Schefer[1], Celia Andreu-Agullo[1], Pui C. Lo[1], Minhee Lee[1], Robert Busby[1], David M. Darst[1], Anne Assmus[1], Suresh Anaganti[2], Nils Halberg[3], Benjamin N. Ostendorf[3], Ivo C. Lorenz[1], Sohail F. Tavazoie[3], Masoud F. Tavazoie[1], and Isabel Kurth[1]

ABSTRACT

MERTK is a receptor tyrosine kinase predominantly expressed on M2 macrophages that plays a critical role in the clearance of apoptotic cells and the maintenance of an immunosuppressive phenotype. M2 macrophages are highly abundant in the tumor microenvironment, in which they facilitate tumor progression and resistance to immunotherapy. MERTK is also overexpressed in cancer cells, in which it can drive cancer survival and metastasis through the induction of proliferation and antiapoptotic signaling programs. In this study, we developed an antibody–drug conjugate (ADC) that simultaneously targets MERTK-expressing M2 tumor-associated macrophages and cancer cells. The ADC comprised the monoclonal antibody RGX-019 that binds human MERTK, combined with a monomethyl auristatin E (MMAE) toxic payload. The unconjugated antibody had intrinsic activity to suppress M2 cytokine expression by macrophages, block *in vitro* colony formation of cancer cells, and inhibit *in vivo* tumor growth and metastasis. When MMAE was conjugated to the antibody, the ADC exhibited superior *in vitro* cytotoxicity and *in vivo* antitumor efficacy in MERTK-expressing tumors. Tumor growth inhibition in humanized mice was associated with the depletion of tumor-associated M2 macrophages. Furthermore, unlike other MERTK-targeting small molecules or antibodies, no retinal toxicity of RGX-019–MMAE was observed *in vivo*. These findings reveal that combined therapeutic targeting of MERTK in cancer cells and M2 macrophages offers enhanced opportunities for antitumor efficacy in a wide range of MERTK-expressing tumors.

Significance: Concomitant targeting of cancer cells and immunosuppressive tumor-associated macrophages with RGX-019-MMAE, a MERTK-targeting antibody-drug conjugate, suppresses tumor growth through direct cancer cell killing and depletion of M2 macrophages.

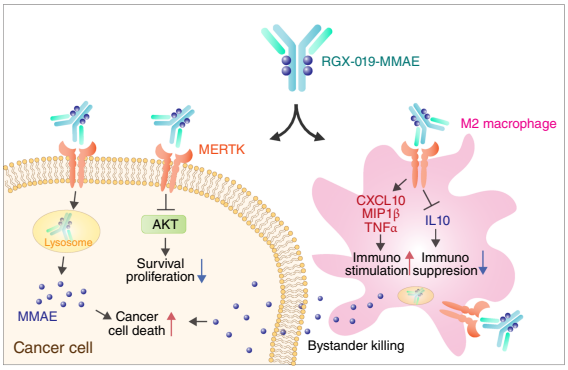

Introduction

MERTK (MER proto-oncogene, tyrosine kinase) is a member of the TAM-R (TYRO3, AXL, and MERTK) family of receptor tyrosine kinases and is most abundantly expressed in innate immune cells, predominantly in tissue and tumor-associated macrophages (TAM) and at lower levels in monocytes and dendritic cells (1). MERTK expression is also observed in activated $CD4^+$ and $CD8^+$ T cells and in regulatory T cells, in which MERTK signaling modulates proliferation (1–3). Furthermore, MERTK expression on endothelial cells regulates endothelial permeability and leukocyte transendothelial migration, and MERTK in retinal pigment epithelium (RPE) cells maintains retinal structure through phagocytic clearance of photoreceptor outer segments (POS; refs. 4, 5).

MERTK on macrophages promotes efferocytosis—the clearance of apoptotic cells—through its interaction with its ligands GAS6 and ProS1, which bridge apoptotic cells to MERTK on macrophages (6). Ligand binding triggers MERTK activation, cytoskeletal rearrangement, and MAPK signaling, which stimulate phagocytosis and the production of anti-inflammatory cytokines (i.e., IL10, VEGF, TGFβ, and arginase-1) that suppress $CD8^+$ T-cell activation and proliferation. In addition, proinflammatory cytokines such as TNFα and IL1β are suppressed by MERTK signaling to avoid an immune response against apoptotic cell-derived self-antigens (7–14). Genetic deletion or small-molecule inhibition of host MERTK in tumor-bearing mice enhances cytotoxic $CD8^+$ T-cell activity in tumors, represses immunosuppression, and induces proinflammatory cytokines (7, 9, 12, 14, 15).

Upregulation of MERTK has also been reported in a wide range of human solid and hematologic cancers (13, 16–24), and its modulation promotes cell proliferation, survival, invasion, metastasis, and drug resistance through ligand-induced MERTK

[1]Inspirna, Inc., Long Island City, New York. [2]L2P Research, Stony Brook, New York. [3]Laboratory of Systems Cancer Biology, The Rockefeller University, New York, New York.

S. Sridhar and D. Schefer contributed equally to this article.

Corresponding Author: Isabel Kurth, 504 E. 63rd Street, New York, NY 10065. E-mail: isabel.kurth@gmail.com

Cancer Res 2026;86:2024–41

doi: 10.1158/0008-5472.CAN-25-2998

autophosphorylation and activation of downstream signaling pathways, including PI3K/AKT, MEK/ERK, and JAK/STAT (25–27).

Thus, within tumors, MERTK contributes to an immunosuppressive environment, tumor progression, and resistance to immunotherapy through modulation of both tumor cells and immunosuppressive myeloid cells. This feature has raised considerable interest as a target for cancer therapeutics. More than 10 small-molecule MERTK inhibitors have entered clinical trials with promising efficacy in preclinical studies. However, many of these small-molecule programs have faced challenges related to off-tumor toxicity caused by poor on-target specificity, and clinical activity remains to be seen (27). Inhibition of MERTK in RPE cells also risks deleterious effects on the retina, an observation made upon treatment with high-dose MERTK-targeting antibodies (15).

To enhance specific cell killing of cancer cells while simultaneously targeting MERTK signaling on M2 macrophages, we developed a highly selective MERTK-directed antibody–drug conjugate (ADC), RGX-019–monomethyl auristatin E (MMAE). ADCs represent a promising class of cancer therapeutics, combining highly cytotoxic small molecules (payloads) with the selective targeting capabilities of antibodies to reduce off-target toxicity and broaden the therapeutic index. RGX-019–MMAE is designed to bind to target antigens on tumor cells and M2 TAMs and release its cytotoxic payloads upon internalization and linker cleavage in the lysosomes. RGX-019–MMAE demonstrates potent antitumor activity in multiple MERTK-expressing xenografts. Additionally, we show that the antibody RGX-019 promotes a proinflammatory cytokine profile in M2 macrophages. *In vivo*, RGX-019–MMAE depletes MERTK-expressing tumoral M2 macrophages, thereby enhancing antitumor immunity. RGX-019–MMAE was well tolerated in mice, with no observed retinal toxicity. Together, our findings support the development of RGX-019–MMAE as a novel ADC with multiple mechanisms of action for the treatment of solid cancers.

Materials and Methods

Cell lines and culture conditions

The cell lines SKMel5 (RRID:CVCL_0527), RPMI-8226 (RRID:CVCL_0014), BT474 (RRID:CVCL_0179), MDA-MB-231 (RRID:CVCL_0062), HL60 (RRID:CVCL_0002), A-427 (RRID:CVCL_1055), NCI-H460 (RRID:CVCL_0459), HepG2 (RRID:CVCL_0027), NCI-H1581 (RRID:CVCL_1479), HPAF-II (RRID:CVCL_0313), and NCI-H358 (RRID:CVCL_1559) were obtained from the ATCC. MDA-MB-231 LM2 cells were generated by *in vivo* selection (16) from the parental cell line MDA-MB-231 (ATCC, RRID:CVCL_0062). MC38-HM (hMERTK-KI) cells were generated by Shanghai Model Organisms (NM-S13-TMMERTK). Certificates of analysis for *Mycoplasma* and pathogen testing were provided by the ATCC and Shanghai Model Organisms. *Mycoplasma* and pathogen testing were conducted by IDEXX BioResearch (h-IMPACT) for the MDA-MB-231 LM2 cells. Cell authentication tests were not performed. Cells were passaged every 2 to 4 days and used at passages <11. SKMel5, RPMI-8226, MC38, MC38-HM, NCI-H1581, NCI-H358, and NCI-H460 were cultured in RPMI 1640 medium (ATCC, 30-2001) containing 10% FBS (Sigma-Aldrich, F2442) and 1% penicillin-streptomycin (Gibco, 15140122). BT474 was cultured in RPMI 1640 medium containing 20% FBS, 10 μg/mL insulin (Gibco, 12585014), and 1% penicillin-streptomycin. MDA-MB-231 and MDA-MB-231-LM2 cells were cultured in DMEM (ATCC, 30-2002) containing 10% FBS and 1% penicillin-streptomycin. HL60 was cultured in Iscove's Modified Dulbecco's Medium (ATCC, 30-2005) containing 20% FBS and 1% penicillin-streptomycin. A427, HepG2, and HPAFII were cultured in Eagle Minimum Essential Medium (ATCC, 30-2003) containing 10% FBS and 1% penicillin-streptomycin.

Animals

All mouse experiments and procedures were approved by the Institutional Animal Care and Use Committees at the New York Blood Center (NYBC), Mispro, and Charles River. huMERTK-KI (C57BL/6Smoc-*MERTK*$^{em1(hMERTK)/Smoc}$) mice were obtained from Shanghai Model Organisms (RRID:IMSR_NM-HU-2000031). MERTK KO (C57BL/6-MERTKtm1Grl/J and Balb/c-Mertk^{tm1Grl}/J) mice were obtained from The Rockefeller University. C57BL/6 (RRID:IMSR_JAX:000664), Balb/c (RRID:IMSR_JAX:000651), athymic nude (RRID:IMSR_JAX:002019), NOD-SCID (RRID:IMSR_JAX:001303), and NOD/SCID gamma (NSG; RRID:IMSR_JAX:005557) mice were obtained from The Jackson Laboratory. Balb/cAnNCrl mice were obtained from Charles River (RRID:MGI:2683685).

MERTK CRISPR knockout cell line

MERTK CRISPR/Cas9 KO and homology-directed repair (HDR) plasmids were obtained from Santa Cruz Biotechnology (sc-401629 and sc-401629-HDR). Five hundred thousand SKMel5 cells were plated in a six-well dish the day prior to transfection and transfected with 2 μg plasmid and Lipofectamine 2000 transfection reagent (Thermo Fisher Scientific, 11668027) diluted in Opti-MEM (Thermo Fisher Scientific, 31985062), according to the manufacturer's instructions. Forty-eight hours after transfection, puromycin selection was initiated at a concentration of 1 μg/mL (Thermo Fisher Scientific, A1113803), and selection was performed for 3 to 5 days by changing to fresh media every 2 to 3 days. Following selection, true MERTK-KO cells were sorted based on the expression of MERTK by flow cytometry. MERTK knockout (KO) was also confirmed via Western blot.

RGX-019 synthesis and generation of RGX-019–MMAE

Mouse IgG1/kappa light chain MERTK-specific monoclonal antibodies were generated in mice by immunization with Fc-tagged human MERTK peptide (R&D Systems, 891-MR-100). Hybridomas were generated from mice that showed MERTK-specific antibodies in serum and were further tested based on a triple screen that included ELISA to measure binding to MERTK, followed by the ability to block GAS6 binding to MERTK, and finally a counter screen for AXL binding. Antibodies from top candidate clones with single-digit nanomolar affinity to MERTK were scaled up in the MAbExpress Bioreactor and further tested in endothelial recruitment assays and *in vivo* antitumor efficacy studies. Antibodies were generated by Antibody Solutions. The clone with the highest specificity, affinity, and activity was then selected for humanization by WuXi Biologics. A human germline sequence with the least number of amino acid differences at counterpart positions in the framework with respect to the murine antibody sequence was selected as the humanization template. A few back mutation sites were selected and combined to constitute various humanized variants. The humanized VH domain was fused to human IgG1 segments in the heavy chain, and the humanized VL domain was fused to the human Ig kappa CK domain in the light chain. The constructs were further codon-optimized for recombinant expression in CHO cells. The

variant with optimal humanization sequence and affinity to MERTK (RGX-019) was chosen for scale-up synthesis using WuXian Express technology. RGX-019 was purified from filtered cell lysates by chromatography on a MabSelect SuRe (50/20) column, followed by a Superdex 200 (50/88) column. Purity was confirmed by SDS-PAGE (>95%) and size-exclusion chromatography (SEC)–high-performance liquid chromatography (100%) analysis. Endotoxin levels were <1 EU/mg. RGX-019 was conjugated with a linker–payload consisting of the microtubule inhibitor MMAE attached to a protease-cleavable linker containing a polyethylene glycol (PEG) spacer group. The antibody was first partially reduced with TCEP-HCl, followed by site-specific cysteine conjugation to the linker–payload, at an average drug-to-antibody ratio (DAR) of 4:1. DAR, purity, and molecular identity of the ADC were confirmed by hydrophobic-interaction chromatography, SEC, and LC-MS analysis, respectively. An isotype control ADC was generated by introducing seven alanine substitutions in the variable heavy chain and one alanine substitution in the variable light chain of RGX-019 and then conjugated to the same MMAE-linker as described above. A version of RGX-019–MMAE with a DAR of 8 was generated using a branched linker and the same technology as described above. A DAR 8 control antibody was generated by attaching the branched linker–payload to motavizumab. Isotype control RGX-019 synthesis and antibody–drug conjugations were conducted by Abzena.

MERTK IHC

Stainings were performed at HistoWiz, Inc. using the Leica BOND RX automated stainer (Leica Microsystems), following a Standard Operating Procedure and a fully automated workflow. A tumor microarray containing 24 human tissues was obtained from Novus Biologicals (NBP2-30170). Tumors from xenograft studies were fixed overnight with 4% paraformaldehyde (PFA; Electron Microscopy Sciences, 50-980-497) at 4°C. After two washes with phosphate-buffered saline (PBS; Gibco, 10010023), tissue was embedded in paraffin following standard protocols. Human peripheral blood mononuclear cells (PBMC), monocytes, and M2 macrophages were fixed overnight with 4% PFA at 4°C. After two washes with PBS, tissue was embedded in paraffin following standard protocols. Human tumor specimens were obtained from Cancer Genetics, Inc., and blocks sectioned into 5-μm-thick sections were mounted on Superfrost Plus Microscope Slides (Fisher Scientific, 22-037-246). Slides were dewaxed using xylene and alcohol-based dewaxing solutions. Epitope retrieval was performed via heat-induced epitope retrieval (HIER) of the formalin-fixed, paraffin-embedded (FFPE) tissue using citrate-based buffer at pH 6 (Leica Biosystems, AR9961) for 20 minutes at 100°C. Endogenous peroxidase activity was blocked using a peroxide block buffer (Leica Biosystems, DS9800). Slides were first blocked for 30 minutes in Background Blocking reagent (Innovex, NB306) before incubation with a rabbit monoclonal MERTK antibody (Abcam, ab52968, RRID:AB_2143584) at a 1:1,000 dilution for 30 minutes, followed by a 60-minute incubation with biotinylated goat anti-rabbit IgG (Vector Labs, PK6101, RRID:AB_2336820) at 5.75 μg/mL, Blocker D. The detection agent diaminobenzidine (DAB Map Staining kit, Roche, 760-124) was used according to the manufacturer's instructions. Slides were counterstained with hematoxylin (Roche, 760-2021) and cover-slipped with Permount (Fisher Scientific, SP15-500) and visualized using an Aperio AT2 slide scanner (Leica Microsystems) at 40× magnification. Tumor proportion score was assessed by a pathologist from three independent fields per specimen.

Hematoxylin and eosin staining

Hematoxylin and eosin (H&E) stainings were performed at HistoWiz, Inc. Samples were prepared in FFPE. Slides were stained using a standard H&E staining protocol (HistoWiz). Slides were then dehydrated, and film was cover-slipped using a Tissue-Tek Prisma and Coverslipper (Sakura Tissue-Tek Film, 4770). Whole-slide scanning (40×) was performed on an Aperio AT2 (Leica Biosystems).

Immunofluorescence for spleen and tonsil

Stainings were performed at the Memorial Sloan Kettering Cancer Center (MSKCC) Flow Cytometry Core Facility. Human tonsil (BioChain, T2234268) and spleen (BioChain, T2234246) were stained by immunofluorescence (IF) for CD68 AF 488+ and MERTK CF 549 as follows: After 32 minutes of heat and Cell Conditioning 1 (Ventana Medical Systems, 950-500) retrieval, the tissue sections were blocked first for 30 minutes in Background Blocking Reagent (Innovex, NB306). A mouse monoclonal anti-CD68 antibody (Abcam, ab303565, RRID:AB_3075482) was used at a 1:1,000 dilution. The incubation with the primary antibody was done for 5 hours, followed by 5.75 μg/mL biotinylated goat anti-mouse secondary (MOM Kit BMK-2202, Vector Labs, RRID:AB_2336833). Blocker D, streptavidin–horseradish peroxidase (HRP) D (part of the DAB Map kit, Ventana Medical Systems), followed by incubation with Tyramide Alexa Fluor 488 (Invitrogen, T20922), was prepared according to the manufacturer's instructions in a 1:150 dilution for 16 minutes. A rabbit monoclonal anti-MERTK antibody (Abcam, ab52968, RRID:AB_2143584) was used at a 1:400 dilution. The incubation with the primary antibody was done for 5 hours, followed by a 60-minute incubation with biotinylated goat anti-rabbit IgG (Vector Lab, PK6101, RRID:AB_2336820) at a 5.75 μg/mL concentration. Blocker D, streptavidin-HRP, and tyramide-CF594 (Biotium, 92174) were prepared according to the manufacturer's instructions in a 1:1,500 dilution for 16 minutes. After staining, slides were counterstained with DAPI (Sigma-Aldrich, D9542, 5 mg/mL) for 10 minutes and mounted with Mowiol (Sigma-Aldrich, 81381). All stainings were performed at the Molecular Cytology Core Facility of MSKCC, using the Discovery XT processor (Ventana Medical Systems, Roche).

IF staining CD68^{+}MERTK + Pan-CK and IHC CD163

Stainings were performed at HistoWiz, Inc., using the Leica BOND RX automated stainer (Leica Microsystems) and a Standard Operating Procedure with a fully automated workflow. Samples were processed, embedded in paraffin, and sectioned at 5 μm. The slides were dewaxed using xylene and alcohol-based dewaxing solutions. Epitope retrieval was performed by HIER of the FFPE tissue using a citrate-based pH 6 solution (Leica Microsystems, AR9961) for 20 minutes at 100°C. The tissues were first incubated with peroxide block buffer (Leica Biosystems, DS9800) and 1× Antibody Diluent/Block (Akoya Biosciences, ARD1001EA) at room temperature for 5 minutes, followed by incubation with the rabbit anti-MERTK antibody (Abcam, ab52968, RRID:AB_2143584) at a 1:1,000 dilution for 40 minutes, rabbit polymer secondary antibody reagents (Bond Polymer Refine Detection Kit, Leica Microsystems, DS9800) for 10 minutes, and Opal 480 tyramide signal fluorescent tag amplified by 1× Plus Automation Amplification Diluent according to the manufacturer's protocol (Akoya Biosciences, FP1500001KT). Primary and secondary antibodies were then stripped with a citrate-based pH 6 solution (Leica Microsystems, AR9961) for 20 minutes at 100°C. Next, the tissues were incubated

with 1× Antibody Diluent/Block (Akoya Biosciences, DS9800), followed by incubation with the mouse anti-panCK antibody (Leica Biosystems, NCL-L-AE1/AE3, RRID:AB_564122) at a 1:100 dilution for 40 minutes, mouse polymer secondary antibody reagents (Leica Biosystems, PV6110, RRID:AB_1307588), and Opal 690 tyramide signal fluorescent tag amplified by 1× Plus Automation Amplification Diluent according to the manufacturer's protocol (Akoya Biosciences, FP1497001KT). Primary and secondary antibodies were again stripped with a citrate-based pH 6 solution (Leica Microsystems, AR9961) for 20 minutes at 100°C. The tissues were incubated with 1× Antibody Diluent/Block (Akoya Biosciences, FP1609), followed by incubation with the rabbit anti-CD68 antibody (Abcam, ab213363, RRID:AB_2801637) at a 1:600 dilution for 40 minutes, rabbit polymer secondary antibody reagents (Bond Polymer Refine Detection Kit, Leica Microsystems, DS9800), and Opal 570 tyramide signal fluorescent tag amplified by 1× Plus Automation Amplification Diluent according to the manufacturer's protocol (Akoya Biosciences). Tissues were counterstained with DAPI (Akoya Biosciences, FP1490), cover-slipped with aqueous mounting media (Leica, CV5030), and visualized using an Akoya Vectra Polaris slide scanner (Akoya Biosciences) at 20×. For costaining with CD163, the slides were first stained for MERTK and CD68 and imaged as described above. After IF scanning was complete, the slides were de-cover-slipped by incubating the slides overnight vertically inside a coplin jar filled with 1× PBS. Next, the tissues were loaded onto the BOND RX and incubated with peroxide block buffer (Bond Polymer Refine Detection Kit, Leica Biosystems, DS9800) for 5 minutes. Following this, the slides were incubated with mouse anti-CD163 (Invitrogen, MA5-11458, RRID:AB_10982556) at a 1:100 dilution for 30 minutes, PowerVision Poly-HRP anti-mouse IgG secondary antibody (Leica Biosystems, PV6114, RRID:AB_1307589) for 8 minutes, DAB Refine for 10 minutes, and hematoxylin for 5 minutes (Bond Polymer Refine Detection Kit, Leica Biosystems, DS9800) according to the manufacturer's instructions. The slides were cover-slipped automatically with a Tissue-Tek Prisma Plus Automated Slide Stainer according to the manufacturer's instructions and were reimaged using the Phenoimager HT fluorescent slide scanner (Akoya Biosciences) at 40× using the bright-field channel. Stainings were conducted on four non–small cell lung cancer (NSCLC) specimens. Forty cells/tumor ($n = 4$ tumors) from three to four random fields were quantified for CD68, MERTK, and CD163 positivity.

Immune cell preparation and differentiation

PBMCs were prepared from buffy coats of healthy donors by Histopaque-1077 (Sigma, 10771) density gradient centrifugation at 250 × *g* at room temperature for 30 minutes. The intermediate layer containing PBMCs was collected, and the cells were washed with PBS containing 2 mmol/L EDTA 3 times. Human monocytes were isolated from PBMCs by magnetic separation using the Human Classical Monocyte Isolation Kit (Miltenyi, 130-117-337) according to the manufacturer's instructions. To differentiate monocytes into M2 macrophages, 2.5×10^5 monocytes were cultured in 24-well plates in RPMI 1640 medium (Gibco, 11875093) containing 10% human AB serum (Sigma, H4522), 10% FBS (Sigma, F2442), L-glutamine, and penicillin-streptomycin (Gibco, 15140122) and M-CSF (50 ng/mL; Miltenyi, 130-096-485) at 37°C with 5% CO_2 for 6 days.

To differentiate monocytes into M1 macrophages, 2.5×10^5 monocytes were cultured in 24-well plates in RPMI 1640 medium containing 10% human AB serum, 10% FBS, L-glutamine, penicillin, and streptomycin and GM-CSF (100 ng/mL; BioLegend, 766102) at 37°C with 5% CO_2 for 4 days. To differentiate monocytes to dendritic cells, 2.5×10^5 monocytes were cultured in 24-well plates in RPMI 1640 medium containing 10% human AB serum, 10% FBS, L-glutamine, penicillin, streptomycin, GM-CSF (100 ng/mL), and IL4 (20 ng/mL; BioLegend, 766202) at 37°C with 5% CO_2 for 5 days. T cells and NK cells were isolated from PBMCs by magnetic separation using the human Pan T Cell Isolation Kit (Miltenyi, 130-096-535) and the NK Cell Isolation Kit (Miltenyi, 130-092-657), respectively, according to the manufacturer's instructions.

Western blot analysis

M2 macrophages *in vitro* differentiated from 2.5×10^5 monocytes were treated with 0.3 μg/mL of RGX-019 for 10 minutes, 30 minutes, 2 hours, 4 hours, 8 hours, and 24 hours. To assess MERTK expression on cancer cells, 3×10^5 SKMel5, 3×10^6 RPMI-8226, and 3×10^5 MDA-MB-231 LM2 cells were cultured in six-well plates overnight and treated with RGX-019 at 0.01, 0.03, 0.1, 0.3, 1, 3, and 10 μg/mL (67 nmol/L) for 24 hours or at 0.3 μg/mL (2 nmol/L) for 10 minutes, 30 minutes, 2 hours, 4 hours, 8 hours, 24 hours, 48 hours, and 72 hours. For the 2 hours, and 24 hours treatment experiment, 3 x 10^5 SKMel5 or 5 x 10^5 BT474 cells were treated with 2 nmol/L of RGX-019 or IgG1 (BioXcell, BP0297, RRID:AB_2687817). For the GAS6 experiment, 1×10^5 SKMel5 cells were cultured in a 24-well plate overnight and treated with 0.3 μg/mL RGX-019 or IgG control (R&D Systems, 1-001-A, RRID:AB_907192) for 2 hours and then stimulated with 200 nmol/L GAS6 (R&D Systems, 885-GSB-050) for 10 minutes. Whole-cell lysates were prepared in RIPA buffer (Sigma, 20-188) containing protease inhibitor (Sigma, 4693159001) and phosphatase inhibitor (Sigma, P2850 and P5726). Protein concentrations were measured using the BCA Protein Assay Kit (Thermo Fisher Scientific, 23225). Equal protein amounts were loaded on 4% to 20% Tris-Glycine gels (Bio-Rad, 4561094) and then transferred to polyvinylidene difluoride membranes (Bio-Rad, 1620177). After blocking with 5% BSA, membranes were incubated in blocking buffer (Bio-Rad, 12010020) for 1 hour with either of the following primary antibodies (1:1,000 dilution): MERTK (Abcam, ab52968, RRID:AB_2143584), phosphorylated MERTK (Abcam, ab14921, RRID:AB_2250636), AKT (Abcam, ab32505, RRID:AB_722681), phosphorylated AKT (Abcam, ab81283, RRID:AB_2224551), β-actin (Sigma, A5316, RRID:AB_476743), or tubulin (Sigma, T5168, RRID:AB_477579) for 1 hour at room temperature. Primary antibodies bound to the membrane were detected with HRP-conjugated secondary antibodies (Sigma, AP187P and AP181P, RRID:AB_92625 and RRID:AB_11214094) and visualized by ECL Western Blotting Substrate (Thermo Fisher Scientific, 32106) using ChemiDoc Imaging Systems (Bio-Rad).

Flow cytometry

Macrophages *in vitro* differentiated from 2.5×10^5 monocytes on 24-well plates were harvested with Cell Dissociation Buffer (Thermo Fisher Scientific, 13151014), washed twice, strained through a 70 μm filter, and resuspended in 200 μL FACS buffer [2% BSA, 10 mmol/L EDTA, 25 mmol/L HEPES (Gibco, 15630080), 0.1% sodium azide (Sigma, S2002-5G) in Ca/Mg-free PBS]. Cells were sequentially stained with BV421-conjugated antibodies against MERTK (BioLegend, 367603, RRID:AB_2566396) for 20 minutes on ice and then stained with Fixable Viability Dye (Thermo Fisher Scientific, 65-0865-14) for 30 minutes on ice. The cells were resuspended in 100 μL of FACS buffer, analyzed with a flow cytometer (BD

LSRFortessa), and the median fluorescence intensity (MFI) of MERTK was obtained from live single cells.

Cytokine production

PBMC-isolated monocytes (see above) were differentiated into M2 macrophages by culturing 2.5×10^5 monocytes in 24-well plates in RPMI 1640 medium (Gibco, 11875093) containing 10% human AB serum, 10% FBS, L-glutamine, penicillin, and streptomycin and M-CSF (50 ng/mL; Miltenyi, 130-096-485) and incubated at 37°C with 5% CO_2 for 5 days. The medium was replaced with serum-free X-VIVO 15 medium (Lonza, 04-418Q) containing M-CSF (50 ng/mL), and cells were cultured for an additional 3 days. Cells were treated with 1 μg/mL RGX-019 or IgG for the past 48 hours of differentiation. For IL10 experiments, the cells were then treated with LPS (20 ng/mL; Sigma, L4391) for 24 hours. Cell culture supernatants were collected and analyzed for IL10 concentrations using a Human IL10 ELISA Kit (Thermo Fisher Scientific, EHIL10) or sent to Eve Technologies, Canada, for Human Cytokine/Chemokine Array (HD42) analysis.

Competitive ELISA affinity assay

Ninety-six–well Nunc MaxiSorp flat-bottom plates (Thermo Fisher Scientific, 44-2404-21) were coated with 0.01 μg/mL human MERTK recombinant protein (R&D Systems, 891-MR-100) overnight at 4°C. Plates were washed 3 times with PBS containing 0.1% Tween (PBST) and blocked with 3% nonfat dry skim milk in PBS for 2 hours. During the saturation step, dilutions of human MERTK, human AXL (R&D Systems, 154-AL-100), human TYRO3 (R&D Systems, 859-DK-100), mouse MERTK (R&D Systems, 591-MR-100), or cynomolgus monkey MERTK (R&D Systems, 10576-MR-050) were prepared at 50 nmol/L as the highest concentration and serially diluted 1:1 to 0.098 nmol/L in PBS. Each dilution of the antigen was incubated with 0.3 nmol/L (for human and monkey MERTK) or 0.6 nmol/L (for human AXL and TYRO3 and mouse MERTK) of RGX-019 at room temperature for 1 hour. Then, the saturated plate was washed 3 times with PBST, and the antigen–antibody mixture was added to the wells in duplicates and incubated for 1 hour at room temperature. The plate was then washed 3 times with PBST and incubated with alkaline phosphatase–conjugated anti-human IgG $F(ab)_2$ antibody (Sigma, SAB3701248) at a dilution of 1:3000 in PBS for 1 hour at room temperature. After washing 3 times with PBST, 100 μL of Alkaline Phosphatase Yellow (pNPP) liquid substrate system (Sigma, P7998) was added to each well and incubated for 70 minutes at room temperature. Absorbance at 405 and 570 nm was measured with the GloMax Discover System (Promega) to correct for plate inconsistencies. The normalized absorbance was plotted as a function of antigen concentration in GraphPad Prism 7.0c. A nonlinear regression curve was drawn using the Bobrovnik affinity equation: $Y = (Amax - Ao) \times [\{sqrt(sqr(X - ABconc + Kd) + 4 \times Kd \times ABconc) - (X - ABconc + Kd)\}/\{2 \times ABconc\}] \times [\{(X + ABconc + Kd)\text{-}sqrt(sqr(X + ABconc + Kd) - 4 \times X \times ABconc)\}/\{2 \times ABconc\}+1](-1)+Ao$, and Kd was calculated (28, 29).

Cell binding assay

RGX-019 and human IgG control (R&D Systems, 1-001-A, RRID:AB_907192) were labeled with the Zenon Allophycocyanin (APC) Human IgG Labeling Kit (Thermo Fisher Scientific, Z25451) according to the manufacturer's instructions. SKMel5 cells were harvested with trypsin-EDTA (Thermo Fisher Scientific, 25200114), washed twice with PBS, and strained through a 70 μm filter. A total of 50,000 cells were resuspended in 60 μL of FACS buffer (2% BSA, 10 mmol/L EDTA, 25 mmol/L HEPES, 0.1% sodium azide in Ca/Mg-free PBS) containing 10% human AB serum (Sigma, H4522). The cells were stained with DAPI (500 ng/mL) and APC-labeled RGX-019 or IgG control for 20 minutes on ice, then washed twice with FACS buffer, and analyzed by flow cytometry (BD LSRFortessa). The APC signal from live single cells was analyzed with FlowJo, and the MFIs were plotted with GraphPad Prism.

MERTK internalization assay

RGX-019 and human IgG control (R&D Systems, 1-001-A, RRID:AB_907192) were labeled with pHrodo Red, a pH-sensitive dye, using the pHrodo Red Microscale Labeling Kit (Thermo Fisher Scientific, P35363) according to the manufacturer's instructions. Internalization of antibody was determined by flow cytometry detecting pHrodo fluorescence, which is minimal at neutral pH and maximal in acidic environments, such as the lysosomes. Twenty thousand SKMel5 cells were plated on 96-well plates and incubated with 67 nmol/L pHrodo-labeled RGX-019 or IgG control antibody for 1, 3, 6, or 24 hours. The cells were harvested with trypsin, washed twice, strained through a 70 μm filter, and resuspended in 100 μL FACS buffer (2% BSA, 10 mmol/L EDTA, 25 mmol/L HEPES, 0.1% sodium azide in Ca/Mg-free PBS). The pHrodo signal was quantified with a flow cytometer (BD LSRFortessa) and analyzed with FlowJo. To capture images of internalized antibodies, 1×10^6 SKMel5 cells were plated on six-well plates and incubated with 6.7 nmol/L pHrodo-labeled RGX-019 or IgG control antibody for 1, 3, 6, or 24 hours. The cells were harvested with Cell Dissociation Buffer (Thermo Fisher Scientific, 13151014), washed twice, strained through a 70 μm filter, and resuspended in 200 μL FACS buffer. Cells were sequentially stained with BV421-conjugated antibodies against MERTK (BioLegend, 367603, RRID:AB_2566396) for 20 minutes on ice and then stained with Fixable Viability Dye (Thermo Fisher Scientific, 65-0865-14) for 20 minutes on ice. A total of 5,000 event multispectral images were acquired for each sample by ImageStream Imaging Flow Cytometer (Amnis). Single-color control samples were used to create a compensation matrix, and the resulting compensated data were analyzed by IDEA software (Amnis) and GraphPad Prism. Internalization of the RGX-019–MMAE was conducted similarly. RGX-019–MMAE and isotype ADC were labeled with pHrodo Red as described above. Fifty thousand SKMel5 or 1×10^5 RPMI-8226 cells were plated on 24-well plates and incubated with 10 nmol/L pHrodo-labeled RGX-019–MMAE and isotype ADC for 6 hours. The cells were trypsinized, washed twice, and resuspended in 100 μL FACS buffer (2% BSA, 10 mmol/L EDTA, 25 mmol/L HEPES, 0.1% sodium azide in Ca/Mg-free PBS). The pHrodo signal was quantified with a flow cytometer (BD LSRFortessa) and analyzed with FlowJo and then normalized by the degree of labeling.

ELISA GAS6 binding assay

PBS was supplemented with 2 mmol/L $CaCl_2$ to facilitate binding between GAS6 and MERTK throughout the study. A 96-well Nunc MaxiSorp flat-bottom plate (Thermo Fisher Scientific, 44-2404-21) was coated with 10 μg/mL human MERTK recombinant protein (R&D Systems, 891-MR-100) in PBS overnight at 4°C and then washed 3 times with PBST. The plate was blocked with 3% nonfat dry skim milk in PBS for 3 hours and washed 3 times with PBST. Dilutions of RGX-019 were prepared at 50 nmol/L as the highest concentration and serially diluted 1:1 to 0.098 nmol/L in PBS. The dilutions of RGX-019 were added to the wells in duplicate, and the

plate was incubated for 2 hours at room temperature and then washed 3 times with PBST. The plate was incubated with 1μg/mL human GAS6 recombinant protein (R&D Systems, 855-GSB-050) for 1 hour at room temperature and then washed 3 times with PBST. Biotin-conjugated anti-His tag antibody (Thermo Fisher Scientific, MA1-21315-BTIN, RRID:AB_2536983) was diluted 1:500 in PBS with 0.1% Tween and 0.1% BSA (PBSTB) and added to the wells. The plate was incubated for 1 hour at room temperature and then washed 3 times with PBST. Streptavidin–alkaline phosphatase (R&D Systems, AR001) diluted at 1:1000 in PBSTB was added, and the plate was incubated for 1 hour at room temperature and then washed 3 times with PBST. The binding of GAS6 was visualized by incubation with PNPP (Sigma, P7998-100ML) for 2 hours at room temperature, and the 405 and 560 nm absorptions were quantified with the Glomax Discover System (Promega). The results were plotted using GraphPad Prism.

Colony formation assay

SKMel5 (500 cells/well), HL60 (500 cells/well), and RPMI-8226 cells (1,000 cells/well) were plated in six-well plates. The cells were treated with 0.3 or 1 μg/mL of IgG control or RGX-019 in triplicates. After 7 days of culture, the media were exchanged for fresh media containing the antibodies at the same concentration. The cells were stained on day 12 (SKMel5, HL60) or day 14 (RPMI-8226). The wells were first washed once with PBS and then stained with 2 mL of 6% glutaraldehyde (v/v) and 0.5% crystal violet (w/v) in PBS for 30 minutes at room temperature. The plates were then rinsed twice by immersing them in a container filled with tap water. They were allowed to dry at room temperature. Once the plates were completely dry, the number of colonies of more than 50 cells was counted by microscopic observation. The results were plotted as a bar graph using GraphPad Prism.

RPE phagocytosis assay

Fifty thousand human RPE cells (Lonza, 194987) were plated on a 24-well plate and cultured in RtEGM medium (Lonza, 195409) for 4 days. The medium was exchanged for RPMI 1640/F-10 supplemented with 2% FBS and cultured for 10 more days to differentiate the cells into fully functional RPE cells. The RPE cells were treated with 1 μg/mL (6.67 nmol/L) or 10 μg/mL (67 nmol/L) RGX-019, control IgG, or 10 μmol/L UNC-1062, a small-molecule MERTK inhibitor, for 2 hours. Bovine POS (InVision BioResources, 98740) was labeled with FITC by incubation in DMEM containing 0.5 mg/mL FITC for 1.5 hours at room temperature. The RPE cells were incubated with FITC-labeled POS at 32 μg/mL for 2 hours to induce phagocytosis of POS. The cells were trypsinized and stained with DRAQ5 (Thermo Fisher Scientific, 65-0880-92) at a dilution of 1:2,500 and analyzed with a flow cytometer (BD LSRFortessa). The frequency of FITC-positive RPE cells was quantified with FlowJo and plotted with GraphPad Prism.

CellTiter-Glo

SKMel5 and SKMel5 CRISPR MERTK-KO cells were harvested with trypsin; diluted to a concentration of 200 cells per 50 μL in RPMI 1640 (ATCC, 30-2001), 10% FBS (Sigma-Aldrich, F2442), and 1% penicillin-streptomycin (Gibco, 15140122); and plated on a 96-well plate. MC38-HM cells were similarly harvested and plated at 200 cells per 50 μL in DMEM (ATCC, 30-2002), 10% FBS (Sigma-Aldrich, F2442), and 1% penicillin-streptomycin (Gibco, 15140122) on a 96-well plate. To differentiate M2 macrophages, 7.5×10^4 monocytes were plated on a 96-well plate in RPMI 1640 medium supplemented with 10% non-heat–inactivated FBS and 1% penicillin-streptomycin (Gibco, 15140122) and 50 ng/mL M-CSF (Miltenyi, 130-096-485). After 24 hours (for SKMel5, SKMel5 MERTK-KO, MC38-HM, or 8-day differentiated M2 macrophages), control IgG1 (BioXCell, BP0297, AB_2687817), isotype-MMAE, RGX-019–MMAE, or free MMAE (R&D Systems, 5683) was diluted to a 2× concentration. A serial dilution of these compounds was performed for a total of 8 dilutions. Fifty microliters of each dilution was added to their respective wells on the 96-well plate. Cells were treated in duplicates with the compounds for a total of 6 (SKMel5, SKMel5 MERTK-KO) or 7 (MC38-HM, M2 macrophages) days. After the incubation period, the CellTiter-Glo 2.0 (Promega, G9241) cell viability assay was performed according to the manufacturer's instructions. Luminescence was read on a GloMax Explorer (Promega, GM3500).

Bystander assay (coculture of MERTK-KO SKMel5 and M2 macrophages)

Human M2 macrophages were differentiated by culturing 2.5×10^5 monocytes isolated from PBMCs, as described above, in 24-well plates in RPMI 1640 medium (Gibco, 11875093) containing 10% FBS, penicillin, and streptomycin and M-CSF (50 ng/mL; Miltenyi, 130-096-485) and incubated at 37°C with 5% CO_2 for 6 days. MERTK-KO SKMel5 cells were labeled with carboxyfluorescein succinimidyl ester (CFSE) dye using the CFSE Cell Division Tracker Kit (BioLegend, 423801) according to the manufacturer's instructions. Ten thousand MERTK-KO SKMel5 cells were then added to the M2 macrophage culture overnight before incubation with 10 nmol/L RGX-019–MMAE or isotype ADC for an additional 6 days in RPMI medium containing 10% FBS and penicillin/streptomycin. The cells were harvested with Accutase (Thermo Fisher Scientific, A1110501) and blocked by incubating with TruStain FcX PLUS (BioLegend, 156603, RRID:AB_2783137) on ice for 10 minutes to reduce background binding mediated by Fc receptors. The cells were resuspended in FACS buffer (1× PBS, 2% FBS, 10 mmol/L EDTA, 0.1% sodium azide, 25 mmol/L HEPES) containing anti-human MERTK antibody (R&D Systems, FAB8912P, RRID:AB_357214) at a dilution of 1:100 and anti-CD163 antibody (Thermo Fisher Scientific, 17-1639-41, RRID:AB_2573167) at a dilution of 1:100 and incubated for 20 minutes on ice. The cells were washed with PBS and stained with Fixable Viability Dye (Thermo Fisher Scientific, 65-0865-14) at a 1:2,000 dilution in PBS for 30 minutes on ice. The cells were washed with FACS buffer and resuspended in 100 μL of FACS buffer containing 10 μL of CountBright beads (Thermo Fisher Scientific, C36950) to be analyzed by flow cytometry (BD LSRFortessa). The absolute numbers of live CFSE-positive MERTK-KO SKMel5 cells and CD163-positive M2 macrophages were calculated from the ratio of events of CountBright beads to cell events.

Biacore binding analysis (surface plasmon resonance)

To assess the binding of antibodies to DDDDK-tagged Mer (Sino Biological, 109143-MM13, RRID:AB_3677048), multicycle kinetic analysis was performed. Kinetic experiments were conducted at 25°C on a Biacore T200 (serial no. 1909913) instrument running Biacore T200 Evaluation Software (Cytiva). HBS-EP+ (Cytiva, BR100669) was used as the running buffer as well as for ligand and analyte dilutions. Antibodies were diluted to 10 μg/mL in the running buffer. At the start of each cycle, antibodies were loaded onto Fc2, Fc3, and Fc4 (active Fcs) on a CM5 precoupled with ~9000 RU anti-Human Fab (Cytiva, 28958325) using standard amine chemistry. IgGs were captured at a flow rate of 10 μL/minute to give an immobilization level (R_L) of ~100 RU. The surface was then allowed to stabilize.

Multicycle kinetic data were obtained using DDDDK-tagged Mer as the analyte, injected at a flow rate of 40 μL/minute. A six-point, twofold dilution range from 200 to 6.25 nmol/L in the running buffer was used. For each concentration, the association phases were monitored for 240 seconds, and the dissociation phase was measured for 800 seconds. Regeneration of the sensor chip surface was conducted between cycles using 10 mmol/L glycine-HCl, pH 2.1 (Cytiva, BR100355). Multiple repeats of a blank and of the DDDDK-tagged Mer antigen were programmed into the kinetic run in order to check the stability of both the surface and analyte over the kinetic cycles. Data were analyzed using a Langmuir (1:1) model with BIAevaluation software (Cytiva). This assay was conducted by Abzena.

Assessment of binding to Fc gamma receptors (surface plasmon resonance)

Binding of test antibodies to high- and low-affinity human Fc gamma receptors was assessed by single-cycle kinetic analysis using a Biacore T200 (serial no. 1909913) instrument running Biacore T200 Evaluation Software (Cytiva) at a flow rate of 30 μL/minute. At the start of each cycle, FcγR (Sino Biological) was captured on a CM5 sensor chip precoupled using a His capture kit (Cytiva, 28995056) with standard amine chemistry.

A five-point, threefold dilution range of test antibody (analyte) without regeneration between each concentration was used for each receptor tested. In all cases, test antibodies were passed over the chip in increasing concentrations, followed by a single dissociation step. Following dissociation, the chip was regenerated with the injection of glycine pH 1.5. The signal from the reference channel Fc1 (blank) was subtracted from that of the Fc loaded with the receptor to correct for differences in nonspecific binding to the reference surface. Data were analyzed using a Langmuir (1:1) model or a steady-state model with BIAevaluation software (Cytiva). The following Fc gamma receptors were obtained from Sino Biological: FcγRIIIA$_{176Phe}$ (10389-H08H), FcγRIIIA$_{176val}$ (10389-H08H1), FcγRIIIB (11046-H08H), FcγRIIA$_{167Arg}$ (10374-H08H), FcγRIIA$_{167His}$ (10374-H08H1), FcγRIIB (10259-H08H), and FcγRI (10256-H08H). This assay was conducted by Abzena.

Assessment of binding to FcRn (surface plasmon resonance)

The binding of the samples to human FcRn (Sino Biological, CT009-H08H) was assessed by multicycle kinetics analysis using a Biacore T200 (serial no. 1909913) instrument running Biacore T200 Evaluation Software (Cytiva) at a flow rate of 30 μL/minute. Human FcRn (Sino Biological) was immobilized onto a CM5 sensor chip (Cytiva) using standard amine chemistry. Samples were titrated in an eight-point twofold dilution from 15.6 to 2000 nmol/L in PBS (Fisher Scientific, 10317052) containing 0.05% polysorbate 20 (P20, Cytiva, BR100054) at pH 6.0 or a three-point twofold dilution from 500 to 2000 nmol/L in PBS containing 0.05% P20 at pH 7.4. Samples were passed over the chip at a flow rate of 30 μL/minute and at 25°C. The injection time was 30 seconds, and the dissociation time was 60 seconds per concentration. Following a single association and dissociation for each concentration of antibody, the chip was regenerated with an injection of 0.1 mol/L Tris pH 8.0. Data were analyzed using a Langmuir (1:1) model with BIAevaluation software (Cytiva). This assay was conducted by Abzena.

In vivo retinal toxicity

Five milligrams per kilogram of IgG1, RGX-019, or RGX-019–MMAE was administered by weekly retro-orbital injection to 9-week-old huMERTK-KI C57/BL6 mice for 4 weeks by intravenous administration ($n = 4$–5). On day 28, the mice were euthanized, and the eyes were collected. As a positive control, an alkylating agent, methyl methanesulfonate (MMS; Fisher Scientific, AC156890050), was administered by a single i.p. injection to 10- to 12-week-old male WT C57BL/6 mice (Charles River) at 75 mg/kg ($n = 4$). The eyes of MMS-treated mice were collected on day 7 after administration. As positive and negative controls, eyes from 3- or 6-month-old male WT C57BL/6 mice and MERTK KO or heterozygous C57BL/6-MERTK^{tm1Grl}/J mice were euthanized, and eyes were collected ($n = 5$). The eyes were fixed in 4% PFS/PBS for 24 hours, processed to FFPE blocks, sectioned in sagittal orientation at a thickness of 5 microns, and stained with H&E. The stained sections were imaged, and the thickness of the outer nuclear layer (ONL) and total thickness of photoreceptor inner segment (IS) and outer segment (OS) from three different areas within a 200 μm distance from the optic nerve were quantified in SlideViewer software (3DHISTECH) as measures of retinal degeneration ($n = 8$–10).

Pharmacokinetic analysis

Pharmacokinetic (PK) evaluation was performed in female NOD-SCID mice (7–8 weeks old, $n = 6$ per group). RGX-019–MMAE was prepared in PBS and administered retro-orbitally at 1, 3, or 10 mg/kg at a volume of 5 mL/kg. Blood samples (~15 μL) were collected directly into EDTA-coated microtainer tubes (BD Biosciences, 365974) from the tail vein or submandibular vein at 2 minutes, 1, 2, 24, 48, 72, 96, and 168 hours after dosing. Plasma was separated by centrifugation for 5 minutes at 2,000 × g. RGX-019–MMAE concentrations were measured using the Human Therapeutic IgG1 ELISA Kit (Cayman Chemical, 500910). WinNonlin (Phoenix, version 8.3 or higher) or other similar software was used for PK calculations.

Metastasis assay

Fifty thousand luciferase-labeled MDA-MB-231 LM2 cells were resuspended in 100 μL of PBS and injected intravenously through tail vein injection in 6-week-old female NSG mice. Treatment with either IgG1 (BioXCell, BP0297, RRID:AB_2687817) or RGX-019 at 10 mg/kg started on the day of inoculation. Dosing occurred twice a week through i.p. injection until the termination of the experiment. Bioluminescence was measured once a week. To measure bioluminescence, 100 μL of D-luciferin (Fisher Scientific, 88292) solution (16.7 mg/mL) in sterile Dulbecco's PBS was injected intraperitoneally. After 2 minutes, mice were imaged in the IVIS Spectrum *In Vivo* Imaging System (PerkinElmer). Photon flux was plotted as the ratio of the bioluminescence signal at a given time point to the signal on day 0.

Primary xenograft tumor growth studies

For primary tumor growth experiments, cancer cells were suspended in 50 μL of PBS and mixed 1:1 with Matrigel (BD Biosciences, 356231) and subcutaneously injected unilaterally or bilaterally into the lower flank of 6- to 11-week-old sex-matched mice. The following cell numbers were injected per inoculation: 2.5×10^6 SKMel5, 10×10^6 RPMI-8226, 2×10^6 MDA-MB 231, 5×10^6 NCI-H1581, 4.2×10^6 NCI-H460, and 5×10^6 BT474. MDA-MB-231 cells were inoculated into the third mammary fat pad of 6-week-old female NOD-SCID mice. For BT474 xenografts, the mice (6–8-week-old female athymic nude) were implanted with 17β-ESTRADIOL pellets (0.5 mg/pellet, 60-day release, Innovative Research of America, SE-121) in the subcutaneous space under the

neck the day before tumor cell inoculation. Upon detection of tumor volumes reaching the size indicated in each figure, mice were randomly assigned to a drug treatment or a control cohort. Isotype human IgG1 control and RGX-019 were administered twice per week. RGX-019–MMAE or isotype-MMAE were administered once per week. For treatment, mice were anesthetized with isoflurane (Covetrus, 309405), and antibodies were injected as indicated in the figures at a volume of 10 mL/kg using a 1 mL Insulin Syringes (EXELINT, 26027). ADCs were diluted in PBS, and antibodies were diluted in sterilized 0.9% NaCl. Body weight and tumor measurements were performed once or twice per week using a digital scale or caliper, respectively. Tumor volume was calculated as follows: (large diameter) × (small diameter)^2/2. The studies were conducted until total tumor volume reached a size of 2,000 mm^3 or an endpoint was determined. Tumor growth inhibition (TGI) was calculated using following the formula: TGI (%) = ((1 − (ΔTi − ΔT0))/(ΔCi − ΔC0)) × 100%. Tumors that were analyzed for MERTK signal were extracted from a separate cohort before tumor volumes reached 1000 mm^3.

Tumor growth and TIL analysis by flow cytometry (huMERTK knock-in C57BL/6 mice)

Two and a half million huMERTK knock-in MC38 cells (MC38-HM, Shanghai Model Organisms) were injected into 11-week-old female huMERTK knock-in C57BL/6 mice (Shanghai Model Organisms) as described above. Upon detection of tumors measuring 160 to 260 mm^3, mice were randomly assigned to each cohort, and treatment with the antibodies, as indicated in the figure, started. On day 6 after administration, the mice were euthanized, and the tumors were collected for flow cytometry studies. The tumors were extracted, minced, and dissociated into single cells using a Tumor Dissociation Kit (Miltenyi, 130-096-730) and a gentleMACS Dissociator (Miltenyi) according to the manufacturer's instructions. CD45$^+$ immune cells were enriched using CD45 microbeads (Miltenyi, 130-052-301) according to the manufacturer's instructions. The cells were resuspended in FACS buffer (1× PBS, 2% FBS, 10 mmol/L EDTA, 0.1% sodium azide, 25 mmol/L HEPES) and blocked by incubating with TruStain FcX PLUS (BioLegend, 156603, RRID:AB_2783137) on ice for 10 minutes to reduce background binding mediated by Fc receptors. The cells were stained with a panel of primary antibodies detecting innate immune cells on ice for 20 minutes. M1 macrophages were defined as CD45$^+$, CD11b$^+$, F480$^+$, MHCII high, CD206$^-$, and M2 macrophages as CD45$^+$, CD11b$^+$, F480$^+$, MHCII low, CD206$^+$ (BioLegend: CD45-BV785, 103149, RRID:AB_2564590; CD11b-BV605, 101237, RRID:AB_11126744; F4/80-FITC, 123107, RRID:AB_893500; MHCII-BV421, 107631, RRID:AB_10900075; CD206-PE-Cy7, 141719, RRID:AB_2562247; MERTK-PE, R&D Systems, FAB8912P, RRID:AB_357214). Following a wash with PBS, the cells were stained with Fixable Viability Dye (Thermo Fisher Scientific, 65-0865-14) on ice for 20 minutes. The cells were washed with FACS buffer and resuspended in 100 to 200 μL of FACS buffer and then analyzed by flow cytometry (BD LSRFortessa). Fluorescence signals from live single cells were analyzed with FlowJo software. Single-color control samples were used to create a compensation matrix.

Tumor growth and TIL analysis of a NSCLC patient-derived xenograft model in humanized mice

Female NOD/Shi-scid/IL2Rγ^{null} immunodeficient mice (Charles River) were engrafted intravenously with cord blood-derived CD34$^+$ hematopoietic stem and progenitor cells (French Blood Bank) 2 days after chemical myeloablative treatment (Busulfan). CD34$^+$ cord blood cells (50,000–100,000 cells intravenously) from three different donors were used and randomized across all groups. Only mice with a humanization rate (hCD45/total CD45) above 25% were used for implantation into the right flank with 5 × 5 × 5 mm tumor fragments of model CTG-0860 (passage 5). A myeloid boost (GM-CSF, IL3, IL4, FLT3L) was performed 1 week after tumor fragment implantation. When the tumors reached 80 to 130 mm^3, mice were randomized into two groups (n = 9) and treated intraperitoneally with control IgG 10 mg/kg twice weekly or RGX-019 10 mg/kg twice weekly. Tumors were extracted on the day of termination, cut into small pieces, and transferred into gentleMACS tubes containing a mix of enzymes. The tumor tissue was then enzymatically digested by running the gentleMACS program according to the manufacturer's instructions. The cell suspension was resuspended in flow cytometry staining buffer. Two million tumor cells were stained and incubated with human FcR blocking reagent (Miltenyi Biotec, 130-059-901) for 5 minutes. Cells were stained with surface antibodies (1:100 dilution) and viability dye together for 30 minutes at 4°C. Antibodies used are as follows: mCD45-BV711 (BioLegend, 103147, RRID:AB_2564383), hCD45-BV510 (BD Biosciences, 304036, RRID:AB_2561940), CD3-BV786 (BD Biosciences, 563800, RRID:AB_2744384), CD163-APC (Miltenyi, 130-112-129, RRID:AB_2655479), CD11b-PE-Cy7 (BioLegend, 301322, RRID:AB_830644), CD14-BV421 (BD Biosciences, 301830, RRID:AB_10959324), and MERTK (R&D Systems, FAB8912P, RRID:AB_357214). This assay was conducted by Champions Oncology.

Tumor growth and TIL analysis by flow cytometry (CT26 in WT and MERTK-KO mice)

Two hundred thousand CT26 cells were inoculated bilaterally into 13- to 17-week-old female WT or MERTK-KO Balb/cAnNcrl mice. Upon detection of tumors measuring 80 to 100 mm^3, mice were randomly assigned to each cohort, and anti–PD-1 (BioXCell, BE0146, RRID:AB_10949053) or isotype rat IgG2a control (BioXCell, BE0089, RRID:AB_1107769) was administered twice a week intraperitoneally at 10 mg/kg. On day 11 after administration, the mice were euthanized, and the tumors were collected for flow cytometry studies. The tumors were extracted, minced, and dissociated into single cells using a Tumor Dissociation Kit (Miltenyi, 130-096-730) and a gentleMACS dissociator (Miltenyi) according to the manufacturer's instructions. The cells were suspended in 35% Percoll (GE HealthCare, 17-0891-01) and layered on 70% Percoll, followed by centrifugation at 2,100 rpm for 20 minutes to enrich TILs by density-gradient separation. The cells were resuspended in FACS buffer (1× PBS, 2% FBS, 10 mmol/L EDTA, 0.1% sodium azide, 25 mmol/L HEPES) and blocked by incubating with TruStain FcX PLUS (BioLegend, 156603, RRID:AB_2783137) on ice for 10 minutes to reduce background binding mediated by Fc receptors. The cells were stained with a panel of primary antibodies detecting innate immune cells on ice for 20 minutes. M1 macrophages were defined as CD45$^+$, CD11b$^+$, F4/80$^+$, MHCII high, and CD206$^-$, and M2 macrophages were defined as CD45$^+$, CD11b$^+$, F4/80$^+$, MHCII low, CD206$^+$ (BioLegend: CD45-BV785, 103149, RRID:AB_2564590; CD11b-BV605, 101237, RRID:AB_11126744; F4/80-FITC, 123107, RRID:AB_893500; MHCII-BV421, 107631, RRID:AB_10900075; CD206-PE-Cy7, 141719, RRID:AB_2562247; MERTK-APC, 151507, RRID:AB_2650738). Following a wash with PBS, the cells were stained with Fixable Viability Dye (Thermo Fisher Scientific, 65-0865-14) on ice for 20 minutes. To determine the activation status of T cells, the enriched TILs were separately suspended in T-cell activation medium (RPMI 1640, 10% FBS,

1× penicillin-streptomycin, 1× L-glutamine, 1× sodium pyruvate, 2× nonessential amino acids, 2.5% HEPES, 50 μmol/L beta-mercaptoethanol) containing a cell activation cocktail (BioLegend, 423303) and incubated for 2.5 hours at 37°C with 5% CO_2. The cells were resuspended in FACS buffer, blocked by incubating with TruStain FcX PLUS on ice for 10 minutes, and stained with a panel of primary antibodies detecting adaptive immune cells on ice for 20 minutes (BioLegend: CD45-BV785, 103149, RRID:AB_2564590; CD3-PerCp Cy5.5, 100217, RRID:AB_1595597; CD4-BV605, 100451, RRID:AB_2564591; CD8a-AF700, eBioscience, 56-0081-82, RRID:AB_494005). Following a wash with PBS, the cells were stained with Fixable Viability Dye on ice for 20 minutes. The cells were suspended in CytoFix/Cytoperm solution (BD, 554722, RRID:AB_2869010) to permeabilize the cells and stained with antibodies against intracellular cytokines (eBioscience, IFNγ-PE-Cy7, 25-7311-82, RRID:AB_469680) in Perm/Wash solution (BD, 554723, RRID:AB_2869011) on ice for 20 minutes. The cells were washed with FACS buffer and resuspended in 100 to 200 μL of FACS buffer and then analyzed by flow cytometry (BD LSRFortessa). Fluorescence signals from live single cells were analyzed with FlowJo software. Single-color control samples were used to create a compensation matrix.

Statistical analysis

All data are expressed as mean ± SEM, unless indicated otherwise. For tumor growth studies, animals were randomly assigned to study cohorts using StudyLog software. The significance of tumor growth curves at termination and flow cytometry data was analyzed using two-tailed *t* tests. Correlation analysis was carried out using simple linear regression. Metastasis assays were analyzed using the nonparametric Mann–Whitney test. The Mantel–Cox log-rank test was used for statistical comparisons in survival analyses. A *P* value less than 0.05 was considered significant. Statistical tests were performed with GraphPad Prism 10.

Results

MERTK is overexpressed in tumors and TAMs

Selective expression of a molecular target in the desired cell populations is a critical requirement for a viable ADC approach. We first assessed MERTK expression in human advanced-stage NSCLC specimens by IHC. Consistent with previous reports, we observed MERTK expression on both tumor-infiltrating immune cells and cancer cells (**Fig. 1A**). Multiplex IF analysis confirmed MERTK expression in $CD68^+$ TAMs and in cancer cells (pan-cytokeratin staining; **Fig. 1B**). At a high level, TAMs are categorized into proinflammatory M1 and immunosuppressive $CD163^+$ M2 TAMs, which, more recently, have also been characterized by the expression of CXCL9 and SPP1, respectively (30, 31). Multiplex IF combined with IHC for CD163 revealed that the majority of $CD68^+$ and $CD163^+$ macrophages in NSCLC specimens colocalize with MERTK expression (83% and 85%, respectively), confirming that MERTK is predominantly expressed on M2-type tumoral macrophages (Supplementary Fig. S1A). Consistently, we observed significantly higher MERTK expression in M2 relative to M1 *in vitro*–differentiated macrophages (**Fig. 1C**; refs. 1, 32). MERTK expression in other immune populations, including human PBMCs, monocytes, NK cells, T cells, *in vitro*–differentiated dendritic cells, and M2 macrophages, also revealed the highest signal in M2 macrophages by Western blot and IHC staining (Supplementary Fig. S1B and S1C).

Analysis of The Cancer Genome Atlas (TCGA) datasets revealed high MERTK mRNA expression in multiple prominent cancers, including renal, lung, glioma, glioblastoma, and thyroid cancers (Supplementary Fig. S1D). However, MERTK signal in these specimens likely stems from several populations, including immune, stromal, and tumor cells. We therefore specifically quantified the expression of MERTK in tumor cells by IHC staining and histopathologic analysis of 111 human advanced-stage tumor specimens from seven solid cancers of high unmet need (melanoma, NSCLC, renal, ovarian, urothelial, pancreatic, and colorectal cancer). The highest expression was seen in ovarian cancer, in which >85% of tumors have a positive MERTK signal, followed by urothelial, NSCLC, and pancreatic cancer (**Fig. 1D** and **E**; Supplementary Fig. S1E).

Toxicity of ADCs is often driven by target expression on normal tissue. We therefore evaluated MERTK expression in 24 healthy organs. We observed three different types of IHC staining: (i) MERTK-negative tissue, (ii) tissue with MERTK-positive immune cells but otherwise negative epithelial staining, and (iii) organs with MERTK-positive epithelial staining at an overall low expression level. Among those, the kidney cortex and medulla showed the highest expression (**Fig. 1F**; Supplementary Fig. S1F). IF staining of the spleen and tonsils confirmed that $CD68^+$ tissue macrophages constitute the major source of MERTK expression in these tissues (**Fig. 1G**). Overall, MERTK's expression profile, with substantial expression in multiple human cancers and M2 TAMs as well as low expression in normal tissue epithelia, suggests an attractive target for an ADC approach.

MERTK degradation and *in vitro* cancer cell killing

RGX-019 is a humanized monoclonal IgG1 antibody that selectively binds to human and cynomolgus monkey MERTK at low nanomolar affinity but not to AXL, TYRO3, or mouse MERTK (Supplementary Fig. S2A to C). To generate an ADC, we attached the potent microtubule inhibitor MMAE to RGX-019 at a DAR ratio of 4 via a cleavable linker and a PEG spacer group to improve solubility (**Fig. 2A**). Notably, surface plasmon resonance (SPR) studies revealed that MMAE conjugation did not alter binding to human FcRn nor Fc gamma receptors (Supplementary Table S1).

Incubation of SKMel5 melanoma cells with low pH-dependent fluorophore pHrodo-labeled RGX-019 caused selective appearance of pHrodo signal in the RGX-019–treated cells, revealing internalization of the antibody and its trafficking to the lysosome (**Fig. 2B** and **C**). Notably, RGX-019 internalization is associated with MERTK depletion from the cell surface (**Fig. 2B**; Supplementary Fig. S2D). Western blot analysis of RGX-019–treated cancer cells confirmed a dose-dependent depletion of total MERTK in multiple cell lines, including SKMel5, MDA-MB-231 triple-negative breast cancer (TNBC), and RPMI-8226 multiple myeloma (**Fig. 2D**; Supplementary Fig. S2E and S2F). To assess the specificity of binding and antigen interaction of the ADC, we developed an isotype control antibody (isotype-MMAE) that harbors the same sequence as RGX-019 except for eight alanine substitutions in the variable domains, which abolished binding to MERTK. pHrodo-labeled RGX-019–MMAE was efficiently internalized in SKMel5 and RPMI-8226 cancer cells, but the labeled isotype control ADC was not, consistent with the lack of MERTK binding (**Fig. 2E**; Supplementary Fig. S2G). The larger SKMel5 cells with higher MERTK expression showed higher levels of internalized RGX-019–MMAE (Supplementary Fig. S2H).

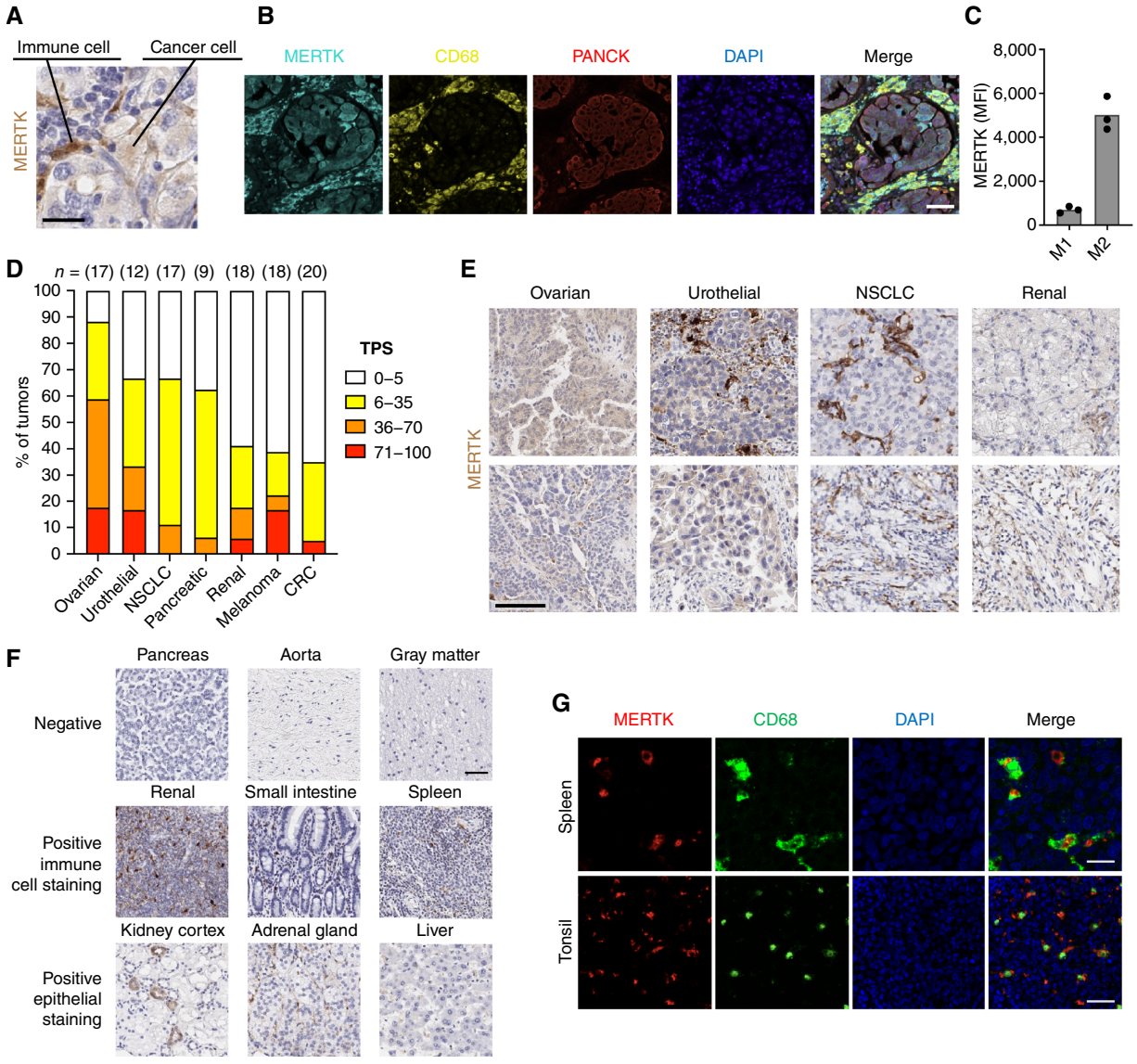

Figure 1.

MERTK expression in cancer and normal tissue. **A** and **B,** IHC (**A**) and IF (**B**) representative images of a human NSCLC tumor specimen for MERTK, macrophages (CD68), cancer cells [pan-cytokeratin (PANCK)], and nuclei (DAPI). Scale bars, 20 μm. **C,** MERTK levels of *in vitro*–differentiated M1 and M2 macrophages by flow cytometry; $n = 3$. **D,** MERTK tumor proportion score (TPS). CRC, colorectal cancer. **E**, Representative images of IHC staining of human tumors. Scale bar, 100 μm. **F,** Representative images of MERTK IHC staining of select tissues from a human tissue microarray. Scale bar, 100 μm. **G,** Representative images of IF analysis for MERTK and CD68 in human spleen and tonsils. Scale bars, 20 and 50 μm, respectively.

We hypothesized that an anti-MERTK ADC would have multiple mechanisms of action, targeting two critical cell populations within tumors: (i) direct cancer cell killing by the toxic payload; (ii) inhibition of MERTK signaling on macrophages to suppress anti-inflammatory cytokines, thereby enhancing antitumor immunity; and (iii) inhibiting MERTK signaling on cancer cells to inhibit proliferation. The combined activity of such a therapeutic may yield greater antitumor responses.

We first evaluated direct cancer cell killing and conducted viability assays in SKMel5 cells. We observed highly potent cell killing by RGX-019–MMAE (GI_{50} = 0.04 nmol/L), which was significantly attenuated in the isotype-MMAE control (**Fig. 2F**). Notably, free MMAE induced similarly efficient cell killing as RGX-019–MMAE, indicating efficient uptake of RGX-019–MMAE and payload release. We also generated a CRISPR SKMel5 MERTK KO cell line, which showed drastically reduced cytotoxicity to RGX-019–MMAE (GI_{50} = 73.2 nmol/L), confirming target-specific cell killing with RGX-019–MMAE (**Fig. 2G**; Supplementary Fig. S2I). Taken together, RGX-019 causes MERTK depletion, and RGX-019–MMAE exhibits potent cytotoxicity in cancer cells in a MERTK-dependent manner.

RGX-019–MMAE induces tumor regressions

Next, we assessed the *in vivo* activity of RGX-019–MMAE across multiple xenografts. PK studies in NOD-SCID animals revealed a

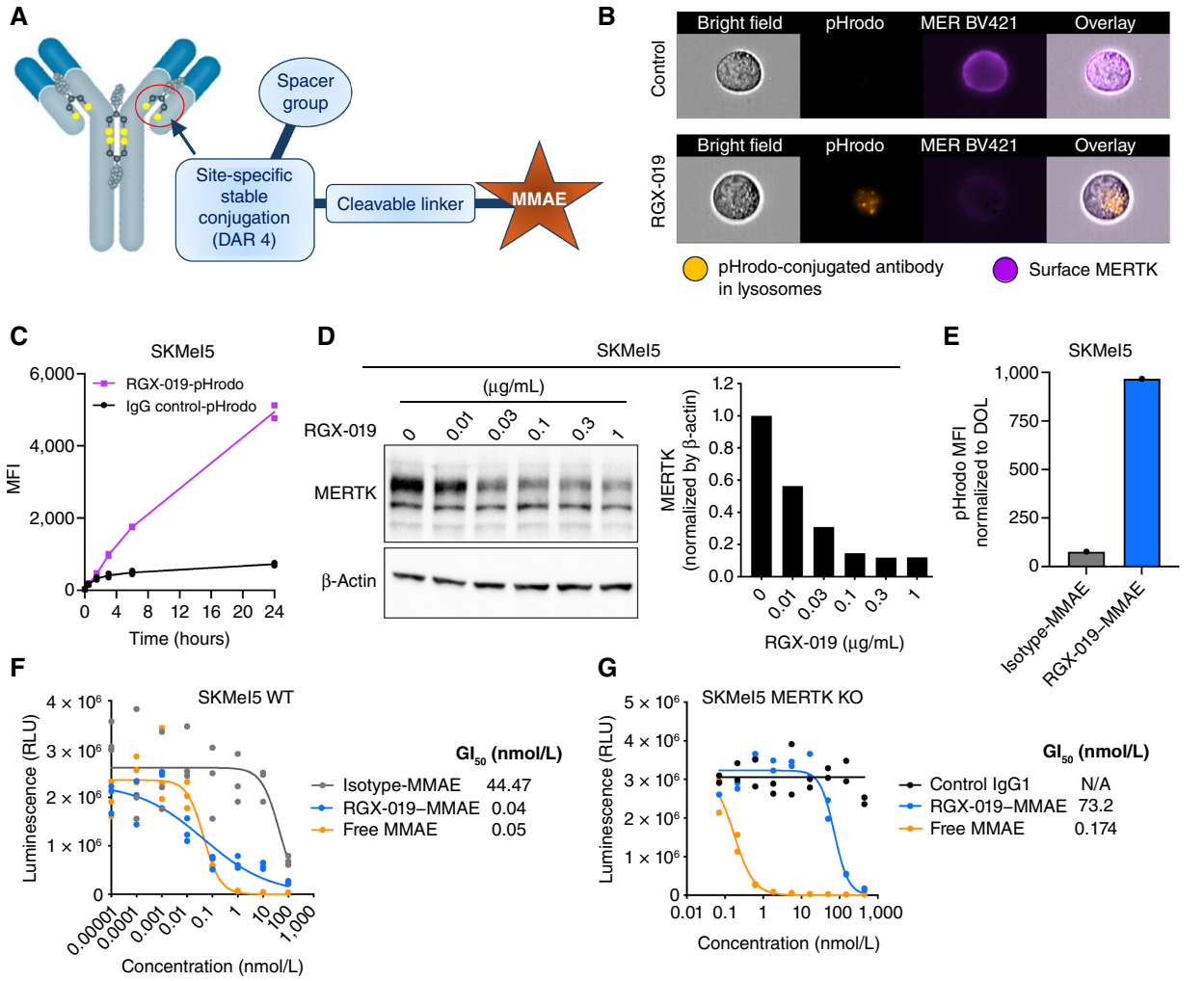

Figure 2.

MERTK degradation and *in vitro* cancer cell killing. **A,** ADC design. **B,** Internalization assay of pHrodo-labeled RGX-019/IgG control in SKMel5 cells, analyzed by imaging flow cytometry. Shown are representative images. **C,** Flow cytometry analysis of SKMel5 cells incubated with pHrodo-labeled RGX-019/IgG control at indicated times (representative of two independent experiments). **D,** Western blot analysis of SKMel5 cells treated with RGX-019 for 24 hours (representative of four independent experiments). **E,** Internalization assay of SKMel5 cells treated with pHrodo-labeled isotype or RGX-019 ADCs for 24 hours; $n = 1$. **F** and **G,** Cell viability of WT (**F**) or CRISPR MERTK KO (**G**) SKMel5 cells incubated with indicated treatments for 7 days; $n = 2$–3.

close to dose-proportional increase in exposure at lower doses, and the mean half-life ranged from 22.9 to 73.6 hours, with half-life increasing at the highest dose (Supplementary Fig. S3A and Supplementary Table S2). In the high MERTK-expressing SKMel5 xenograft, RGX-019–MMAE exhibited dose-dependent antitumor efficacy, with tumor regressions seen in 9/9 tumors at 5 mg/kg and substantially prolonged survival (**Fig. 3A**). Tumor regressions and survival benefits were also observed in RPMI-8226 tumors, which did not respond to treatment with the unconjugated antibody alone (**Fig. 3B**). We also observed sensitivity to RGX-019–MMAE in models with lower MERTK expression, including the MDA-MB-231 TNBC model, in which all tumors (10/10) regressed (**Fig. 3C**). Only modest antitumor efficacy was observed in the low MERTK-expressing NCI-H1581 xenograft (**Fig. 3D**) and the MERTK-negative NSCLC model NCI-H460 was resistant to RGX-019–MMAE, as expected (**Fig. 3E**).

Studies to address target-specific TGI using SKMel5 MERTK-KO cells were challenging as these tumors did not grow well, consistent with MERTK's tumor-promoting role. We thus utilized the isotype control ADC and found that treatment with RGX-019–MMAE caused significantly more TGI compared with the isotype-MMAE (**Fig. 3F**) in WT SKMel5 tumors. However, we did observe partial target-independent antitumor efficacy (**Fig. 3F**; Supplementary Fig. S3B and S3C). SPR binding studies confirmed that the isotype control did not bind MERTK, excluding the possibility of residual target interaction (Supplementary Fig. S3D). However, we observed an 11% loss of the payload within 96 hours in mouse serum. In contrast, the construct was stable in human serum, suggesting that a mouse-specific release of the payload could explain the partial antitumor efficacy observed *in vivo* for the isotype-MMAE ADC (Supplementary Fig. S3E). Overall, these studies demonstrate that RGX-019–MMAE confers direct tumor cell killing *in vivo*.

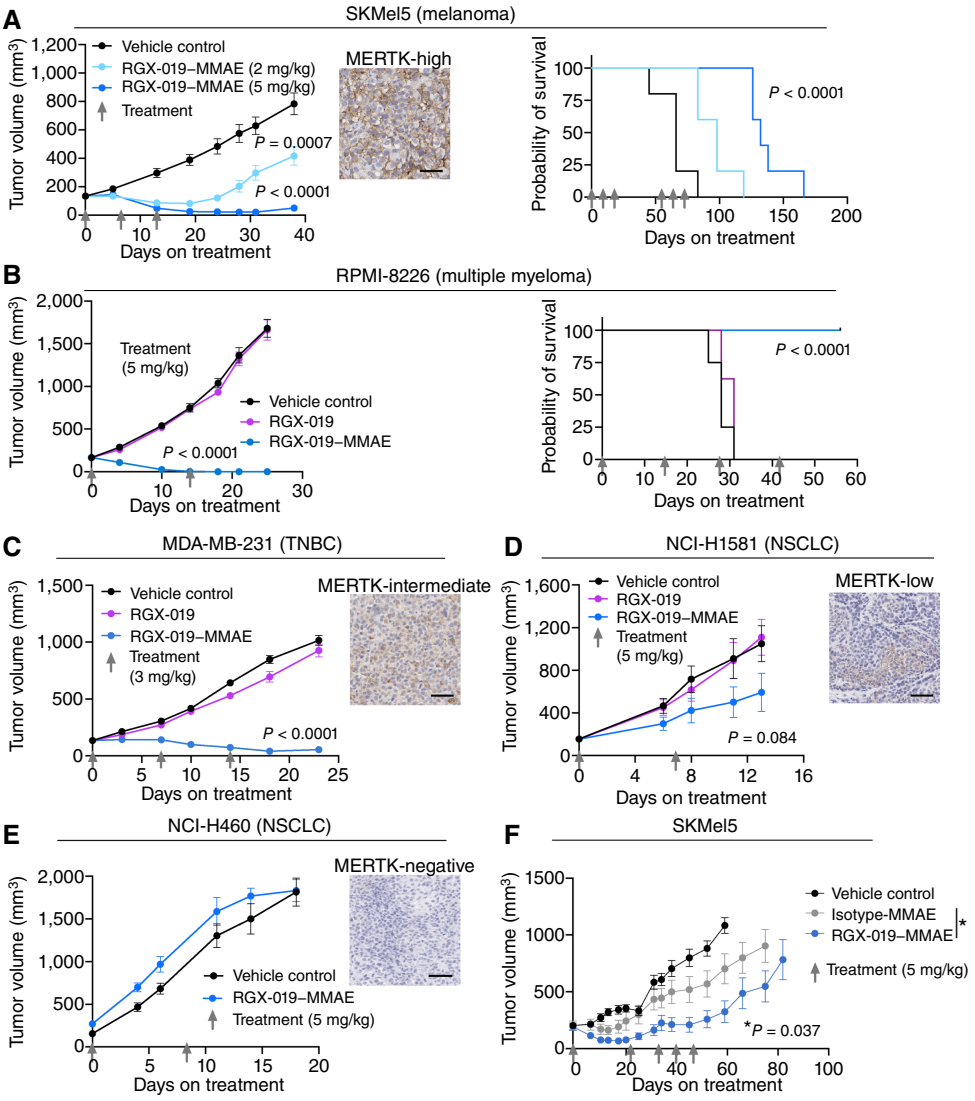

Figure 3.

RGX-019–MMAE induces tumor regressions. **A,** Tumor growth and Kaplan–Meier survival curves of SKMel5 cells in NSG mice. Retro-orbital injections of vehicle or RGX-019–MMAE started when tumors reached ~150 mm^3; n = 9–10 tumors/cohort. Insets in **A**, **C**, **D**, and **E**, representative MERTK IHC staining of control tumors. Scale bars, 50 μm. **B,** Tumor growth and Kaplan–Meier survival curves of RPMI-8226 cells in NOD-SCID mice. Weekly tail vein injections with vehicle control or RGX-019–MMAE started when tumors reached ~170 mm^3; n = 8–9 tumors/cohort. **C,** Tumor growth of MDA-MB-231 in NOD-SCID mice. Tail vein injections of indicated treatments started when tumors reached ~130 mm^3; n = 10 tumors/cohort. **D** and **E,** Tumor growth of NCI-H1581 (**D**) or NCI-H460 (**E**) cells in athymic nude mice. Retroorbital injections of indicated treatments started when tumors reached ~180 mm^3; n = 6–10 tumors/cohort. **F,** Tumor growth of SKMel5 cells in NSG mice. Retroorbital injections of indicated treatments started when tumors reached ~200 mm^3; n = 7–10 tumors/cohort. *, $P = 0.037$.

RGX-019 modulates antitumor immunity

To assess antitumor efficacy mediated by host MERTK (i.e., on M2 TAMs), as opposed to direct cancer cell killing, we used a knock-in transgenic WT mouse model that expresses chimeric MERTK consisting of a human MERTK extracellular domain (huMERTK) and a mouse MERTK transmembrane/intracellular domain. RGX-019, which does not bind mouse MERTK, can bind the human extracellular domain, and the mouse intracellular domain mediates subsequent downstream signaling. For consistency, we also used a mouse colon cancer MC38 cell line with the same human/mouse MERTK (MC38-HM). MC38 cells are known to be MMAE-resistant due to ABCB1 expression, which functions as an MMAE efflux pump (33). Viability assays confirmed low cell killing of the MC38-HM cells, even with an ADC version that harbors eight instead of four MMAE per antibody (DAR 8) to increase cytotoxicity (Supplementary Fig. S4A). RGX-019–MMAE significantly inhibited MC38-HM syngeneic tumor growth in the huMERTK knock-in mice (**Fig. 4A**). Importantly, antitumor efficacy was also observed with the nonconjugated antibody RGX-019 at higher doses, suggesting that the antibody portion of the construct substantially contributes to the antitumor efficacy. In contrast, neither RGX-019 nor RGX-019–MMAE caused TGI of MC38-HM tumors in WT mice (**Fig. 4B**). These findings indicate that tumor inhibition in these mice is largely mediated by the activity of RGX-019 against huMERTK expressed in the host animals, possibly through modulating MERTK-expressing macrophages.

To test this hypothesis, we analyzed the distribution of M1 and M2 TAMs in the MC38-HM tumors upon treatment with both the unconjugated antibody and the ADC. Both RGX-019 and RGX-019–MMAE significantly diminished M2 TAM levels, whereas M1 TAMs remained unaffected (**Fig. 4C**).

We then turned to a NSCLC patient-derived xenograft model in $CD34^+$ humanized mice (**Fig. 4D**). Compared with the control IgG1-treated cohort, we observed significant inhibition of tumor growth in the RGX-019–treated animals (**Fig. 4E**). Tumor-infiltrating lymphocyte (TIL) analysis revealed that RGX-019 diminished the abundance of $MERTK^+$ M2 TAMs (**Fig. 4F**), which strongly correlated with tumor volumes and tumoral $CD3^+$ T cells

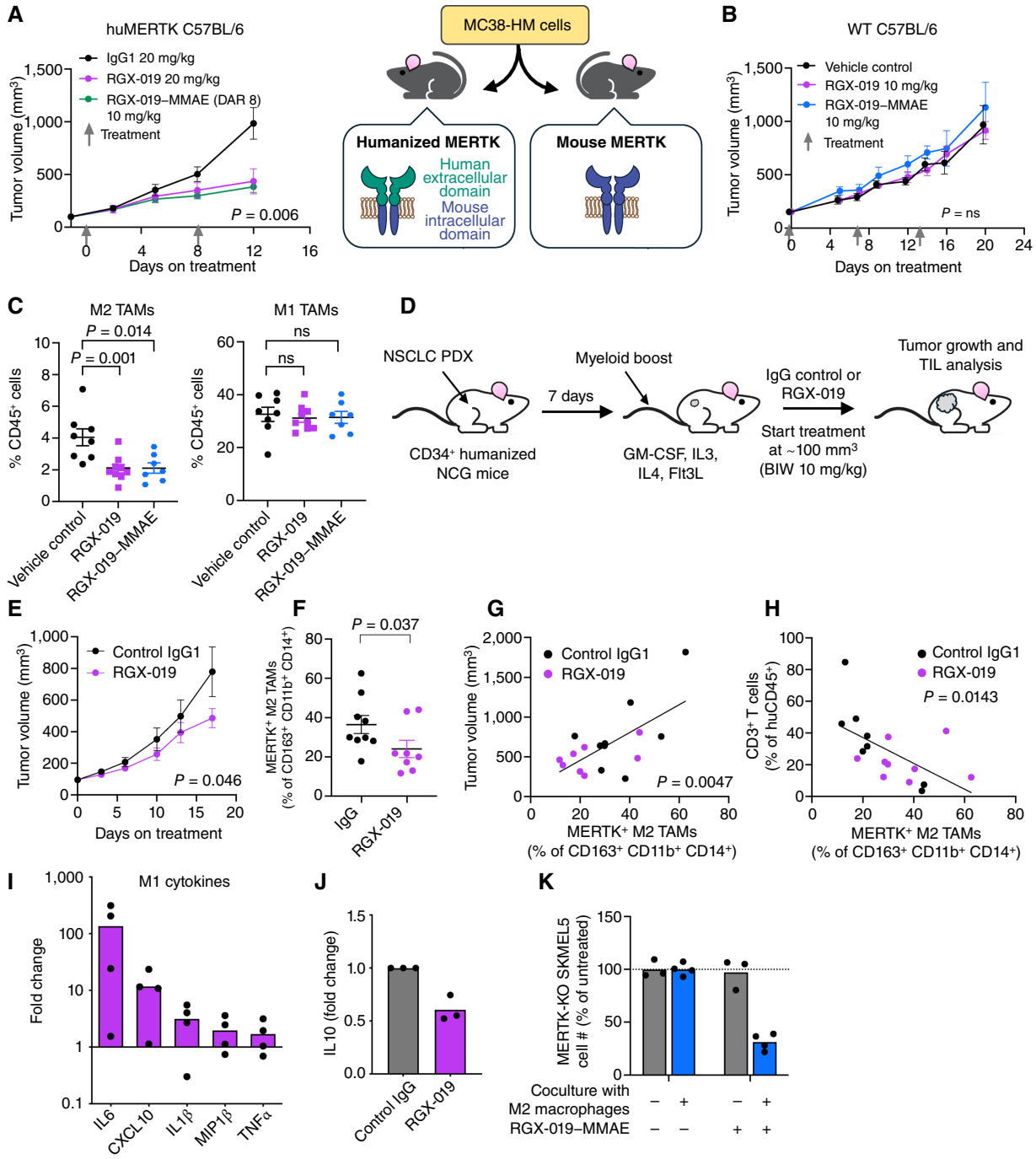

Figure 4.

RGX-019 modulates antitumor immunity. **A** and **B,** Primary tumor growth of MC38-HM cells expressing chimeric human/mouse MERTK in huMERTK (**A**) or WT (**B**) C57BL/6 mice. Retroorbital injections of indicated treatments started at ~150 mm^3 tumor volume; $n = 7$–9 tumors/cohort. **C,** MC38-HM cells were injected subcutaneously into huMERTK knock-in mice. One retroorbital dose of RGX-019 or RGX-019–MMAE was given when tumors reached ~200 mm^3. On day 6, TILs were analyzed for M2 (MHCII-low, $CD206^+$) and M1 (MHCII-high, $CD206^-$) macrophages by flow cytometry; $n = 7$–9. **D–H,** CTG-0860 NSCLC patient-derived xenograft (PDX) fragments were inoculated into $CD34^+$ humanized NOD/Shi-scid/$IL2R\gamma^{null}$ immunodeficient (NCG) mice. One week later, the mice received a myeloid boost (GM-CSF, IL3, IL4, Flt3L). Treatment with control IgG1 or RGX-019 at 10 mg/kg twice weekly (BIW; i.p.) started when tumors reached ~100 mm^3. **E,** Primary tumor growth; $n = 9$ tumors/cohort. **F,** Tumors were extracted at termination, and $MERTK^+$ M2 TAMs were analyzed by flow cytometry; $n = 8$–9. **G,** Correlation analysis of tumor volume and $MERTK^+$ M2 TAMs. **H,** of $CD3^+$ T cells and $MERTK^+$ M2 TAMs. **I,** Cytokine levels of *in vitro*–differentiated M2 macrophages treated with 1 μg/mL RGX-019/IgG control for 48 hours by multiplex LASER bead; $n = 4$. **J,** IL10 levels of *in vitro*–differentiated M2 macrophages treated with 1 μg/mL control IgG1 or RGX-019 by ELISA; $n = 3$. **K,** *In vitro*–differentiated M2 macrophages were cocultured with CFSE-labeled MERTK-KO SKMel5 cells with isotype-MMAE or RGX-019–MMAE for 6 days. Viability of MERTK-KO SKMel5 cells was quantified by flow cytometry; $n = 3$–4.

(**Fig. 4G** and **H**). Tumors with higher levels of MERTK$^+$ M2 TAMs were generally larger and had fewer CD3$^+$ T cells.

We also assessed the effects of RGX-019 *in vitro*. Treatment of M2 macrophages with RGX-019 caused depletion of total MERTK, similar to cancer cells (Supplementary Fig. S4B), confirming target engagement. Furthermore, we observed increased production of proinflammatory cytokines IL6, CXCL10, IL1β, MIP1β, and TNFα (**Fig. 4I**). LPS is a strong activator of macrophages that induces anti-inflammatory cytokines (34). RGX-019 inhibited LPS-mediated induction of IL10 in M2 macrophages (**Fig. 4J**), revealing that RGX-019 modulates macrophage cytokine profiles toward a proinflammatory phenotype.

These effects are consistent with previous data reporting increased tumor inhibition and antitumor immunity in the context of MERTK depletion or pharmacologic inhibition. Furthermore, various studies have reported enhanced TGI in combination with checkpoint inhibitors (27, 35–38). Consistent with these findings, we observed increased TGI of anti–PD-1 treatment against CT26 colorectal tumors in MERTK KO compared with WT animals, accompanied by depletion of tumoral M2 macrophages and an increase in IFNγ$^+$ CD8$^+$ T cells in these tumors (Supplementary Fig. S4C–S4F). These data support RGX-019–MMAE as a promising candidate for future studies in combination with checkpoint inhibitors.

RGX-019–MMAE is efficiently internalized by macrophages but is not expected to kill them as they are not considered highly proliferative (Supplementary Fig. S4G and S4H). However, we wondered whether RGX-019–MMAE can mediate bystander killing, a mechanism of killing neighboring cells upon extracellular release of the payload. We cultured CFSE-labeled MERTK-KO SKMel5 cells with *in vitro*–differentiated M2 macrophages. Treatment with RGX-019–MMAE robustly diminished MERTK-KO SKMel5 cells by 69% only when cocultured with M2 macrophages, demonstrating effective M2 macrophage-mediated bystander killing (**Fig. 4K**). This effect could explain the equivalent antitumor efficacy that we observed in **Fig. 4A**, in which RGX-019–MMAE was dosed at half the dose of the unconjugated antibody.

In summary, our data suggest that RGX-019–MMAE's ability to modulate cytokine expression, as well as mediate bystander efficacy by macrophages, might enhance the antitumor effects of the ADC beyond direct cancer cell killing.

Intrinsic antitumor activity of RGX-019

We next sought to understand the activity of the antibody itself. In cancer cells, MERTK signaling mediates MERTK dimerization and autophosphorylation, followed by activation of downstream signaling (27). We found that the binding of RGX-019 to SKMel5 cells induced transient MERTK and AKT phosphorylation (**Fig. 5A**) with a peak seen within 10 minutes, indicative of pathway activation. ELISA experiments also revealed that RGX-019 blocks GAS6 binding to MERTK (Supplementary Fig. S5A) and prevents GAS6-induced activation of AKT (**Fig. 5B**), suggesting that RGX-019 has partial transient agonist activity. Several small-molecule kinase inhibitors have been developed to block MERTK signaling, but they often lack specificity and harbor safety risks, including retinal toxicity (39, 40). Here, we demonstrate that RGX-019 can inhibit ligand-induced signaling but acts through a distinct mechanism, via transient activation of MERTK, followed by antibody/MERTK internalization and MERTK depletion (**Figs. 2B** and **5A** and **B**).

To assess whether MERTK modulation translates into antitumor activity, we conducted *in vitro* colony formation assays. RGX-019 inhibited the colony formation of SKMel5, RPMI-8226, and HL60 (AML) cancer cells (**Fig. 5C**; Supplementary Fig. S5B; ref. 19).

In vivo activity of RGX-019 was evaluated in multiple primary xenografts. There was modest inhibition of SKMel5 tumor growth and tumoral MERTK depletion upon RGX-019 treatment (**Fig. 5D** and **E**). MERTK depletion was also observed in the low MERTK-expressing A427 NSCLC xenograft although no TGI was seen (Supplementary Fig. S5C and S5D). In contrast, RGX-019 completely inhibited the growth of BT474 breast cancer tumors compared with the vehicle control (**Fig. 5F**). Surprisingly, MERTK levels in this cell line were much lower than in the SKMel5 (Supplementary Fig. S5E); however, we observed highly elevated levels of baseline pMERTK, indicating continuous activation of this pathway that might suggest enhanced dependency on MERTK signaling for survival (Supplementary Fig. S5E and S5F). Previous work demonstrated that MERTK promotes breast cancer metastasis (16, 24). We thus investigated RGX-019's activity on lung colonization of human MDA-MB-231-LM2 TNBC cells and observed 47% inhibition of metastasis in the RGX-019–treated animals compared with the IgG control (**Fig. 5G**).

Overall, although we observed target engagement and MERTK depletion by RGX-019 *in vivo*, antitumor efficacy is likely dependent on multiple factors, including MERTK expression and baseline MERTK activation. These findings, therefore, support an ADC approach to enhance tumor killing, whereas RGX-019's intrinsic activity may contribute to the overall efficacy of RGX-019–MMAE.

Retinal safety

Targeting MERTK has raised concerns of ocular toxicity, as MERTK plays a role in the phagocytosis of shed POSs to support healthy POS renewal (5). In humans, mutations in MERTK are associated with retinitis pigmentosa, an inherited retinal disorder that causes vision loss due to damaged photoreceptor cells (41). To assess the risk for retinal degeneration, we treated human RPE cells with RGX-019 or a small molecule MERTK kinase inhibitor, UNC-1062, and added FITC-labeled bovine POS to drive POS phagocytosis. RGX-019 inhibited POS phagocytosis by 27% compared with untreated cells (**Fig. 6A**). Higher concentrations of RGX-019 did not further increase inhibition, suggesting a plateauing effect. In contrast, UNC-1062 inhibited POS phagocytosis by 73%, indicating that RGX-019 does not completely inhibit the function of MERTK in RPE-mediated phagocytosis, possibly because RGX-019 does not completely deplete MERTK or its activity in these cells.

To evaluate retinal toxicity *in vivo*, we treated huMERTK mice with RGX-019, RGX-019–MMAE, or IgG1 control by weekly dosing. On day 28, the eyes were collected for histologic analysis. As a positive control, an alkylating agent, MMS, was administered to WT mice. MMS-treated animals or MERTK KO mice displayed severe retinal degeneration, with significantly reduced thickness of the ONL and photoreceptor IS, and OS (**Fig. 6B** and **C**; ref. 42). Neither administration of RGX-019 nor RGX-019–MMAE caused any visible effect on the thickness of these layers (**Fig. 6B** and **D**). Given our observation that RGX-019 only partially inhibits *in vitro* phagocytosis of POS cells (**Fig. 6A**), we sought to determine whether reduced expression of MERTK is sufficient to maintain healthy retinal homeostasis. Indeed, three- or six-month-old heterozygous MERTK KO mice showed normal retinal structures, in contrast to the homozygous MERTK KO mice, which displayed severe retinal degeneration (Supplementary Fig. S6A and S6B),

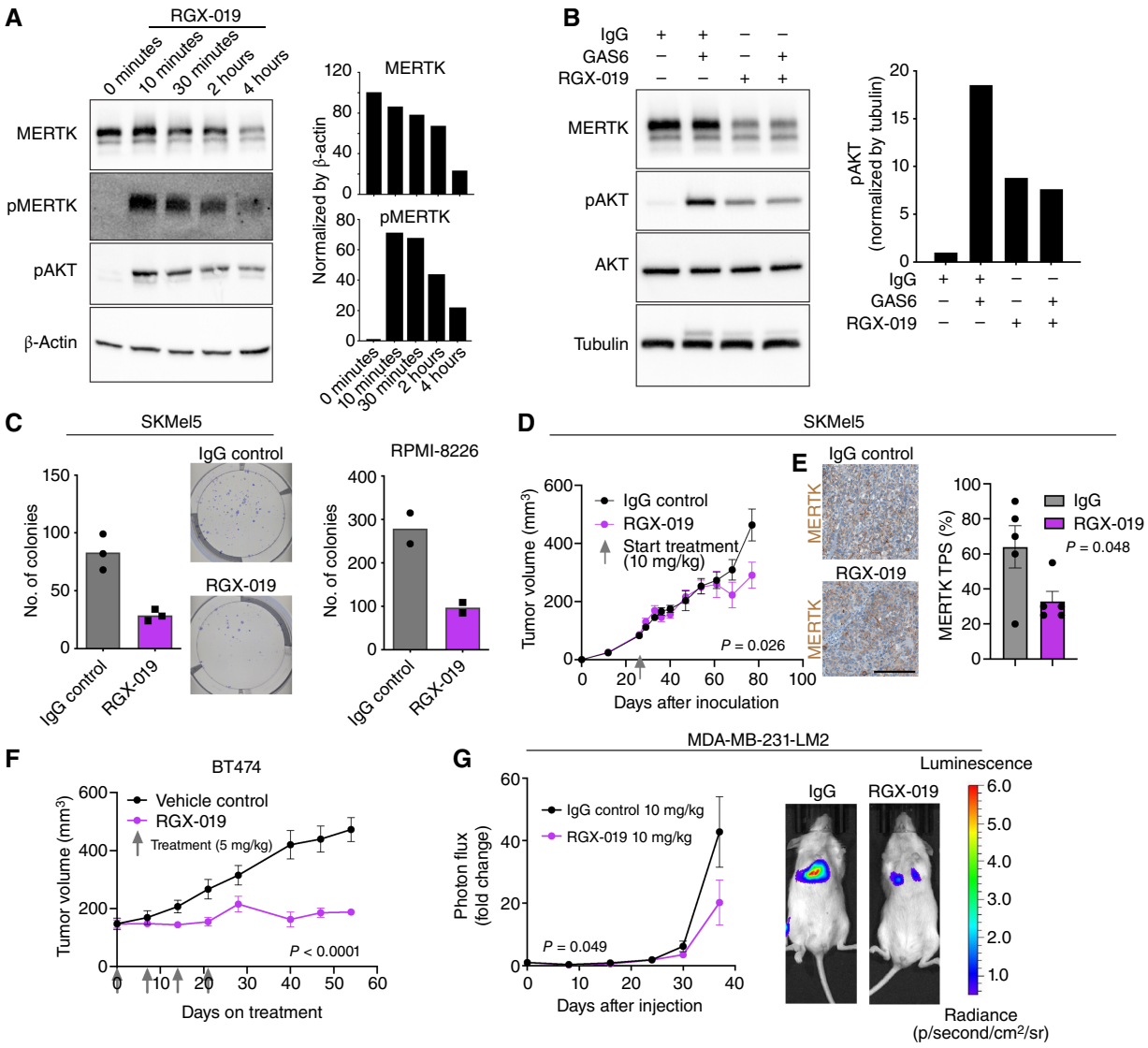

Figure 5.

Intrinsic antitumor activity of RGX-019. **A,** Western blot analysis of SKMel5 cells treated with 0.3 μg/mL RGX-019 or IgG control for MERTK, phosphorylated MERTK (pMERTK), and phosphorylated AKT (pAKT); $n = 1$. **B,** Western blot analysis of SKMel5 cells treated with 2 nmol/L RGX-019 or IgG control for 2 hours, then stimulated with 200 nmol/L GAS6 for 10 minutes (representative of two independent experiments). **C,** Representative images of the colony formation assay with SKMel5 or RPMI-8226 cells incubated with 1 μg/mL RGX-019 or IgG control for 12 ($n = 3$) or 14 days ($n = 2$), respectively. **D,** Tumor growth of SKMel5 cells in NOD-SCID mice. Treatment with control IgG or RGX-019 twice/week i.p. started when tumors reached ~80 mm^3; $n = 8$–10 tumors/cohort. **E,** Representative images of MERTK IHC and tumor proportion score (TPS) of the tumors from **D**. Scale bars, 200 μm; $n = 5$. **F,** Primary tumor growth of BT474 cells in athymic nude mice. Retroorbital dosing of control IgG or RGX-019 started when tumors reached ~150 mm^3; $n = 5$–6 tumors/cohort. **G,** Lung metastasis assay of luciferase-labeled MDA-MB-231 LM2 cells injected into the tail vein of NSG mice. Retroorbital injections twice/week started the day of cell injection; $n = 7$ mice/cohort. Representative images are shown.

indicating that even an approximately 50% reduction of MERTK expression is sufficient to maintain normal MERTK function in the retina (43). Furthermore, RPE cells are not expected to be sensitive to MMAE, given that they are fully differentiated and not proliferative. Taken together, our findings reveal partial inhibition of phagocytosis by RPE upon RGX-019 treatment and no notable signs of retinal toxicity with RGX-019 or RGX-019–MMAE in huMERTK mice. The ADC was also well tolerated, without signs of body weight loss (Supplementary Fig. S6C). However, safety studies in appropriate toxicology models will be needed to assess potential risks, including retinal, renal, or bone marrow toxicity, in detail.

Overall, we report the development of a potent MERTK-targeting ADC. We demonstrate that this ADC mediates direct cancer cell killing both *in vitro* and *in vivo*, as well as inhibition of MERTK signaling in cancer cells and macrophages, in addition to suppression of anti-inflammatory cytokines and depletion of M2 macrophages in tumors via its antibody-intrinsic activity. We propose a model whereby targeting MERTK provides additional

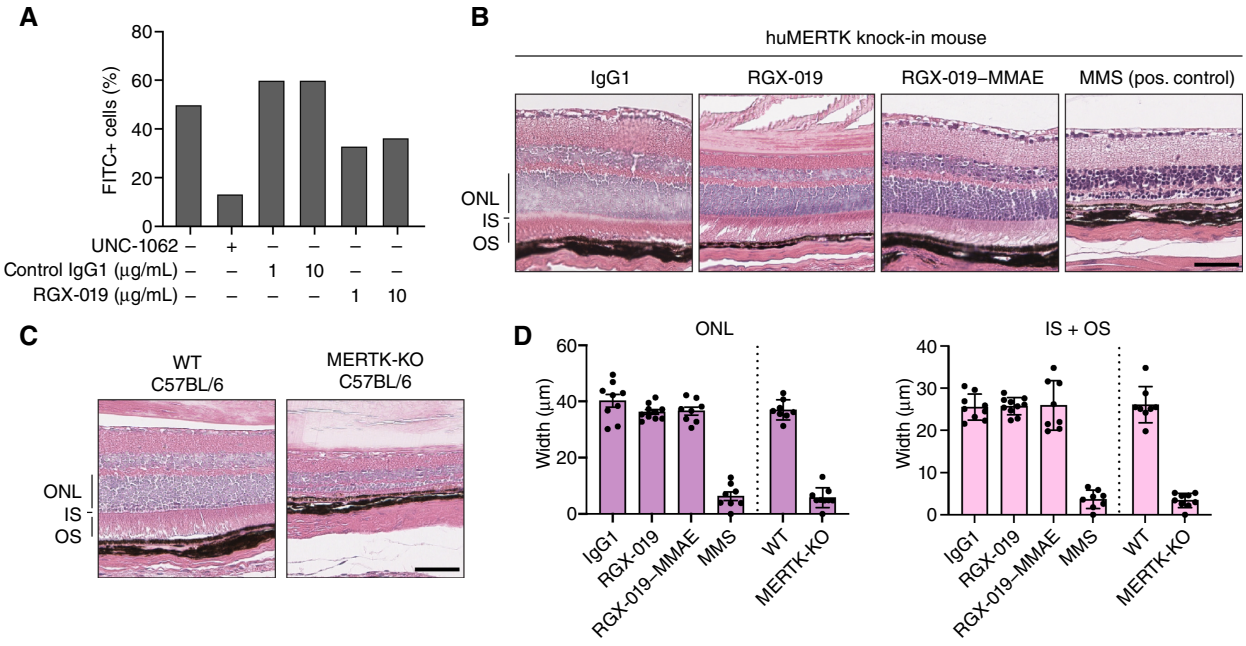

Figure 6.

Retinal safety. **A,** *In vitro*–differentiated primary human RPE cells were treated with indicated concentrations of IgG1, RGX-019, or UNC-1062 (10 μmol/L) for 2 hours, before incubation with FITC-labeled bovine POS for 1 to 2 hours, followed by flow cytometry (representative of two independent studies). **B,** huMERTK mice were treated with weekly IgG1, RGX-019, or RGX-019–MMAE retroorbital injections (5 mg/kg) for 28 days. Eyes were collected for H&E staining. One cohort received a single dose (75 mg/kg) of an alkylating agent MMS. ONL and photoreceptor IS and OS; $n = 8$–10/cohort. Scale bars, 50 μm. **C,** Eyes from WT and MERTK KO C57BL/6 mice were collected as in **B**. **D,** Quantification of the indicated retinal layers.

benefits in heterogeneous and macrophage-rich tumors through a combination of direct cancer cell killing and suppression of MERTK-mediated modulation of TAMs.

Discussion

TAMs are one of the most abundant immune cell populations in solid tumors and can comprise up to 30% to 50% of the tumor mass (**Fig. 1A** and **B**; Supplementary Fig. S1A; refs. 44, 45). Most TAMs are anti-inflammatory M2-type macrophages, in which responses are modulated by multiple processes, including increased tumor cell apoptosis or cytokines and growth factors released by tumor cells (8, 46). The abundance of M2 macrophages has also been shown to inversely correlate with patient survival, thus generating significant interest in therapeutically targeting this population (47, 48). Multiple strategies have been pursued, including depleting TAMs by inhibition of CSF1R, reprogramming M2 to M1 macrophages (CD40, TLR7/8, PI3Kγ), inhibiting recruitment (CCR2, CXCR4), or enhancing phagocytosis (CD46; ref. 48). Despite advancements into clinical development, success has been modest and often accompanied by off-target and on-target toxicities related to the expression of the target in healthy cell populations.

Interest in MERTK as a new therapeutic approach for targeting TAMs is based on its high expression in M2 TAMs and its anti-inflammatory roles (**Figs. 1** and **4**; ref. 27). MERTK inhibition by small-molecule inhibitors or antibodies has shown a shift toward an IFNI response in macrophages and the inhibition of downstream MERTK signaling, accompanied by TGI. Combination treatment with checkpoint inhibitors further enhanced tumor inhibition, supporting the idea that the antitumor activity of immunotherapies can be improved by concomitantly targeting MERTK (Supplementary Fig. S4; refs. 27, 31, 35–38). MERTK is also overexpressed in many tumors, offering a distinctive opportunity for a dual mechanism of action that can directly target cancer cells and the antitumor immune response. We show that MERTK expression is highly specific to cancer cells and immune cells, predominantly M2-type macrophages, with low expression in normal epithelia, which is of particular importance for ADC approaches (**Fig. 1**).

Among the various MERTK-targeting approaches, including kinase inhibitors, therapeutic antibodies, protein degraders, and inhibitors of ligand–receptor interactions, several programs have entered clinical trials (27). The dual small-molecule inhibitor targeting MERTK and FLT3 (MRX-2843) is the most advanced program, currently in phase II clinical studies (49, 50). Results from these trials remain to be reported, but targeting MERTK signaling may be challenging given that alternative TAM-R family kinases (AXL or TYRO3) could mediate compensatory signaling. Tumors may also upregulate other growth factors as a resistance mechanism. Indeed, our studies reveal that MERTK inhibition on cancer cells by RGX-019 results in limited antitumor efficacy (**Fig. 3**).

ADCs have emerged as powerful tools to deliver potent cytotoxic agents to target-expressing cells by utilizing antibodies as vehicles. We, therefore, designed an anti-MERTK ADC that substantially increased tumor cell killing relative to the unconjugated antibody. We observed robust TGI and regression responses by RGX-019–MMAE in multiple models, including models with heterogeneous and reduced MERTK expression (**Fig. 3**). Importantly, we find that the macrophage-modulating features of RGX-019 are maintained in the ADC. Both a humanized *in vivo* tumor model and a transgenic mouse model expressing MERTK with a human extracellular

domain were sensitive to RGX-019 treatment. In both models, we observe that tumors treated with RGX-019 or RGX-019–MMAE contain fewer M2 macrophages and that T-cell levels in the huMERTK mouse are inversely correlated with the abundance of M2 macrophages (**Fig. 4**). Notably, our data suggest that RGX-019–MMAE might be a promising candidate to complement checkpoint inhibitors for increased antitumor efficacy. However, as RGX-019 does not bind to mouse MERTK, it is difficult to assess the full potential for antitumor activity in the context of both targeting cancer cells and TAMs. Additional studies in refined humanized models would be needed to assess the maximum efficacy and the optimal dosing paradigm.

Although small-molecule and antibody programs have demonstrated promising preclinical activity, retinal toxicity concerns have been raised (15). Our studies revealed that neither the unconjugated antibody nor the ADC induces retinal toxicity in mice *in vivo*. Instead of completely blocking MERTK signaling, we found that RGX-019 induces initial activation of MERTK, followed by its depletion. This partial agonistic activity and surface expression might be sufficient to maintain phagocytic activity in the retina, a hypothesis consistent with our findings that heterozygous animals, with lower levels of MERTK, do not show retinal defects (**Fig. 6**).

Overall, our data provide support for the development of a MERTK-targeting ADC that offers opportunities for targeting two critical tumor populations: cancer cells and TAMs.

Data Availability

All raw data generated in this study are available upon request from the corresponding author. The gene expression data analyzed in this study were obtained from cBioPortal using the TCGA pan-cancer dataset.

Authors' Disclosures

S. Takeda reports other support from Phrontline Biopharma outside the submitted work and a patent for US20240279347A1 Mertk peptides and uses thereof pending and a patent for US12281174B2 High-affinity anti-MERTK antibodies and uses thereof issued. S. Sridhar reports other support from Arcus Biosciences outside the submitted work. C. Andreu-Agullo reports a patent for PCT/US2020/019690 issued to Inspirna. D.M. Darst reports a patent for PCT/US2015/067118 pending and issued to Rockefeller University. N. Halberg reports a patent for "Anti-MERTK agonistic antibodies and uses thereof" issued. I.C. Lorenz reports a patent for "High-affinity anti-MERTK antibodies and uses thereof" pending. S.F. Tavazoie reports personal fees from Inspirna during the conduct of the study as well as personal fees from Inspirna outside the submitted work and a patent for MERTK antagonist licensed to Inspirna. M.F. Tavazoie reports personal fees and other support from Inspirna during the conduct of the study and a patent for PCT/US15/067118 issued, licensed, and with royalties paid from Inspirna; a patent for PCT/US18/39445 issued and licensed to Inspirna; a patent for PCT/US2020/019690, 16/801,078 issued; and a patent for PCT/US2022/029185 pending. I. Kurth reports a patent for PCT/US2020/019690 issued and a patent for PCT/US2022/029185 pending. No disclosures were reported by the other authors.

Authors' Contributions

S. Takeda: Conceptualization, data curation, formal analysis, supervision, investigation, methodology, writing–original draft, writing–review and editing. **S. Sridhar:** Formal analysis, validation, methodology, writing–review and editing. **D. Schefer:** Formal analysis, validation, methodology, writing–review and editing. **C. Andreu-Agullo:** Data curation, formal analysis, supervision, validation, investigation, visualization, methodology. **P.C. Lo:** Formal analysis, validation, methodology. **M. Lee:** Data curation, formal analysis, methodology. **R. Busby:** Data curation, software, formal analysis. **D.M. Darst:** Conceptualization, resources, funding acquisition. **A. Assmus:** Resources, funding acquisition, investigation. **S. Anaganti:** Investigation, methodology. **N. Halberg:** Conceptualization, data curation, supervision, methodology, writing–review and editing. **B.N. Ostendorf:** Conceptualization, data curation, supervision, methodology, writing–review and editing. **I.C. Lorenz:** Supervision, investigation, methodology, writing–review and editing. **S.F. Tavazoie:** Conceptualization, resources, formal analysis, supervision, funding acquisition, writing–review and editing. **M.F. Tavazoie:** Conceptualization, resources, data curation, formal analysis, supervision, funding acquisition, investigation, writing–review and editing. **I. Kurth:** Conceptualization, resources, data curation, formal analysis, supervision, validation, investigation, visualization, writing–original draft, project administration, writing–review and editing.

Acknowledgments

We are grateful to Ijeoma Obi; Drs. Darren Wong, Amish Patel, and Foster Gonsalves; and members of our laboratories for help with figures and insightful comments. We thank Drs. Usman "Oz" Azam and Robert Lutz for suggestions and guidance, Yingbei Chen for tumor pathologic assessment, the teams at HistoWiz, and Afsar Barlas (Memorial Sloan Kettering Cancer Center) for immunostainings; Louise Woolley (Champions Oncology) for the humanized mouse study; and WuXi Biologics and Drs. Nicolas Camper and Arron Hearn (Abzena) for antibody/ADC synthesis/characterization. S.F. Tavazoie was supported by an NCI R35 Outstanding Investigator Award CA274446, an NCI MetNet CA261701 award, the Black Family Center for Human Metastasis, and the Marlene Hess Center for Research on Women's Health and Biomedicine.

Note

Supplementary data for this article are available at Cancer Research Online (http://cancerres.aacrjournals.org/).

Received July 11, 2025; revised November 19, 2025; accepted February 2, 2026; posted first February 9, 2026.

References

1. Giroud P, Renaudineau S, Gudefin L, Calcei A, Menguy T, Rozan C, et al. Expression of TAM-R in human immune cells and unique regulatory function of MerTK in IL-10 production by tolerogenic DC. Front Immunol 2020;11:564133.
2. Wallet MA, Sen P, Flores RR, Wang Y, Yi Z, Huang Y, et al. MerTK is required for apoptotic cell-induced T cell tolerance. J Exp Med 2008;205:219–32.
3. Cabezón R, Carrera-Silva EA, Flórez-Grau G, Errasti AE, Calderón-Gómez E, Lozano JJ, et al. MERTK as negative regulator of human T cell activation. J Leukoc Biol 2015;97:751–60.
4. Li Y, Wittchen ES, Monaghan-Benson E, Hahn C, Earp HS, Doerschuk CM, et al. The role of endothelial MERTK during the inflammatory response in lungs. PLoS One 2019;14:e0225051.
5. Mazzoni F, Safa H, Finnemann SC. Understanding photoreceptor outer segment phagocytosis: use and utility of RPE cells in culture. Exp Eye Res 2014;126:51–60.
6. Scott RS, McMahon EJ, Pop SM, Reap EA, Caricchio R, Cohen PL, et al. Phagocytosis and clearance of apoptotic cells is mediated by MER. Nature 2001;411:207–11.
7. Bosurgi L, Bernink JH, Delgado Cuevas V, Gagliani N, Joannas L, Schmid ET, et al. Paradoxical role of the proto-oncogene Axl and Mer receptor tyrosine kinases in colon cancer. Proc Natl Acad Sci U S A 2013;110:13091–6.
8. Christofides A, Strauss L, Yeo A, Cao C, Charest A, Boussiotis VA. The complex role of tumor-infiltrating macrophages. Nat Immunol 2022;23:1148–56.
9. Cook RS, Jacobsen KM, Wofford AM, DeRyckere D, Stanford J, Prieto AL, et al. MerTK inhibition in tumor leukocytes decreases tumor growth and metastasis. J Clin Invest 2013;123:3231–42.
10. Davra V, Kumar S, Geng K, Calianese D, Mehta D, Gadiyar V, et al. Axl and Mertk receptors cooperate to promote breast cancer progression by combined oncogenic signaling and evasion of host Antitumor immunity. Cancer Res 2021;81:698–712.
11. Huelse JM, Fridlyand DM, Earp S, DeRyckere D, Graham DK. MERTK in cancer therapy: targeting the receptor tyrosine kinase in tumor cells and the immune system. Pharmacol Ther 2020;213:107577.
12. Kasikara C, Davra V, Calianese D, Geng K, Spires TE, Quigley M, et al. Pan-TAM tyrosine kinase inhibitor BMS-777607 enhances Anti-PD-1 mAb efficacy

in a murine model of triple-negative breast cancer. Cancer Res 2019;79:2669–83.
13. Wu YM, Robinson DR, Kung HJ. Signal pathways in up-regulation of chemokines by tyrosine kinase MER/NYK in prostate cancer cells. Cancer Res 2004;64:7311–20.
14. Yokoyama Y, Lew ED, Seelige R, Tindall EA, Walsh C, Fagan PC, et al. Immuno-oncological efficacy of RXDX-106, a novel TAM (TYRO3, AXL, MER) family small-molecule kinase inhibitor. Cancer Res 2019;79:1996–2008.
15. White KF, Rausch M, Hua J, Walsh KH, Miller CE, Wells CE, et al, MERTK-specific antibodies that have therapeutic antitumor activity in mice disrupt the integrity of the retinal pigmented epithelium in cynomolgus monkeys. Cancer Res 2019;79(Suppl 13):558.
16. Png KJ, Halberg N, Yoshida M, Tavazoie SF. A microRNA regulon that mediates endothelial recruitment and metastasis by cancer cells. Nature 2011;481:190–4.
17. Brandao LN, Winges A, Christoph S, Sather S, Migdall-Wilson J, Schlegel J, et al. Inhibition of MerTK increases chemosensitivity and decreases oncogenic potential in T-cell acute lymphoblastic leukemia. Blood Cancer J 2013;3:e101.
18. Lee-Sherick AB, Eisenman KM, Sather S, McGranahan A, Armistead PM, McGary CS, et al. Aberrant Mer receptor tyrosine kinase expression contributes to leukemogenesis in acute myeloid leukemia. Oncogene 2013;32:5359–68.
19. Linger RM, Lee-Sherick AB, DeRyckere D, Cohen RA, Jacobsen KM, McGranahan A, et al. Mer receptor tyrosine kinase is a therapeutic target in pre-B-cell acute lymphoblastic leukemia. Blood 2013;122:1599–609.
20. Xie S, Li Y, Li X, Wang L, Yang N, Wang Y, et al. Mer receptor tyrosine kinase is frequently overexpressed in human non-small cell lung cancer, confirming resistance to erlotinib. Oncotarget 2015;6:9206–19.
21. Schmitz R, Valls AF, Yerbes R, von Richter S, Kahlert C, Loges S, et al. TAM receptors Tyro3 and Mer as novel targets in colorectal cancer. Oncotarget 2016;7:56355–70.
22. Kim JE, Kim Y, Li G, Kim ST, Kim K, Park SH, et al. MerTK inhibition by RXDX-106 in MerTK activated gastric cancer cell lines. Oncotarget 2017;8:105727–34.
23. Yi JH, Jang J, Cho J, Do IG, Hong M, Kim ST, et al. MerTK is a novel therapeutic target in gastric cancer. Oncotarget 2017;8:96656–67.
24. Iida M, Crossman BE, Kostecki KL, Glitchev CE, Kranjac CA, Crow MT, et al. MerTK drives proliferation and metastatic potential in triple-negative breast cancer. Int J Mol Sci 2024;25:5109.
25. Linger RM, Keating AK, Earp HS, Graham DK. TAM receptor tyrosine kinases: biologic functions, signaling, and potential therapeutic targeting in human cancer. Adv Cancer Res 2008;100:35–83.
26. Tibrewal N, Wu Y, D'Mello V, Akakura R, George TC, Varnum B, et al. Autophosphorylation docking site Tyr-867 in Mer receptor tyrosine kinase allows for dissociation of multiple signaling pathways for phagocytosis of apoptotic cells and down-modulation of lipopolysaccharide-inducible NF-kappaB transcriptional activation. J Biol Chem 2008;283:3618–27.
27. Tanim KM, Holtzhausen A, Thapa A, Huelse JM, Graham DK, Earp HS. MERTK inhibition as a targeted novel cancer therapy. Int J Mol Sci 2024;25:7660.
28. Friguet B, Chaffotte AF, Djavadi-Ohaniance L, Goldberg ME. Measurements of the true affinity constant in solution of antigen-antibody complexes by enzyme-linked immunosorbent assay. J Immunol Methods 1985;77:305–19.
29. Bobrovnik SA. Determination of antibody affinity by ELISA. Theory. J Biochem Biophys Methods 2003;57:213–36.
30. Bill R, Wirapati P, Messemaker M, Roh W, Zitti B, Duval F, et al. CXCL9: SPP1 macrophage polarity identifies a network of cellular programs that control human cancers. Science 2023;381:515–24.
31. Wu N, Li J, Li L, Yang L, Dong L, Shen C, et al. MerTK$^+$ macrophages promote melanoma progression and immunotherapy resistance through AhR-ALKAL1 activation. Sci Adv 2024;10:eado8366.
32. Mohd Idrus FN, Ahmad NS, Hoe CH, Azlan M, Norfuad FA, Yusof Z, et al. Differential polarization and the expression of efferocytosis receptor MerTK on M1 and M2 macrophages isolated from coronary artery disease patients. BMC Immunol 2021;22:21.
33. Hingorani DV, Allevato MM, Camargo MF, Lesperance J, Quraishi MA, Aguilera J, et al. Monomethyl auristatin antibody and peptide drug conjugates for trimodal cancer chemo-radio-immunotherapy. Nat Commun 2022;13:3869.
34. Rossol M, Heine H, Meusch U, Quandt D, Klein C, Sweet MJ, et al. LPS-induced cytokine production in human monocytes and macrophages. Crit Rev Immunol 2011;31:379–446.
35. Cruz Cruz J, Allison KC, Page LS, Jenkins AJ, Wang X, Earp HS, et al. Inhibiting efferocytosis reverses macrophage-mediated immunosuppression in the leukemia microenvironment. Front Immunol 2023;14:1146721.
36. Huelse JM, Bhasin SS, Jacobsen KM, Yim J, Thomas BE, Branella GM, et al. MERTK inhibition selectively activates a DC - T-cell axis to provide anti-leukemia immunity. Leukemia 2024;38:2685–98.
37. Lee-Sherick AB, Jacobsen KM, Henry CJ, Huey MG, Parker RE, Page LS, et al. MERTK inhibition alters the PD-1 axis and promotes anti-leukemia immunity. JCI Insight 2018;3:e97941.
38. Zhou Y, Fei M, Zhang G, Liang WC, Lin W, Wu Y, et al. Blockade of the phagocytic receptor MerTK on tumor-associated macrophages enhances P2X7R-dependent STING activation by tumor-derived cGAMP. Immunity 2020;52:357–73.e9.
39. Sayama A, Okado K, Yamaguchi M, Samata N, Imaoka M, Kai K, et al. The impact of the timing of dosing on the severity of UNC569-Induced ultrastructural changes in the mouse retina. Toxicol Pathol 2020;48:669–76.
40. Hamm G, Maglennon G, Williamson B, Macdonald R, Doherty A, Jones S, et al. Pharmacological inhibition of MERTK induces in vivo retinal degeneration: a multimodal imaging ocular safety assessment. Arch Toxicol 2022;96:613–24.
41. Parinot C, Nandrot EF. A comprehensive review of mutations in the MERTK proto-oncogene. Adv Exp Med Biol 2016;854:259–65.
42. Nomura-Komoike K, Nishino R, Fujieda H. Effects of different alkylating agents on photoreceptor degeneration and proliferative response of Muller glia. Sci Rep 2024;14:61.
43. Duncan JL, Yang H, Vollrath D, Yasumura D, Matthes MT, Trautmann N, et al. Inherited retinal dystrophy in Mer knockout mice. Adv Exp Med Biol 2003;533:165–72.
44. Gentles AJ, Newman AM, Liu CL, Bratman SV, Feng W, Kim D, et al. The prognostic landscape of genes and infiltrating immune cells across human cancers. Nat Med 2015;21:938–45.
45. Li C, Yu X, Han X, Lian C, Wang Z, Shao S, et al. Innate immune cells in tumor microenvironment: a new frontier in cancer immunotherapy. iScience 2024;27:110750.
46. Hourani T, Holden JA, Li W, Lenzo JC, Hadjigol S, O'Brien-Simpson NM. Tumor associated macrophages: origin, recruitment, phenotypic diversity, and targeting. Front Oncol 2021;11:788365.
47. Jung KY, Cho SW, Kim YA, Kim D, Oh BC, Park DJ, et al. Cancers with higher density of tumor-associated macrophages were associated with poor survival rates. J Pathol Transl Med 2015;49:318–24.
48. Liu M, Liu L, Song Y, Li W, Xu L. Targeting macrophages: a novel treatment strategy in solid tumors. J Transl Med 2022;20:586.
49. Steuer C, Carlisle J, Leal T, Ardeshir F, Holmes M, Schneider F, Chen Z, et al. A phase 1b Study of the MER tyrosine kinase inhibitor, MRX-2843, in combination with osimertinib in advanced EGFR mutant non-small cell lung cancer. J Thorac Oncol 2024;19:S196.
50. Nakamura R, Yamada T, Tokuda S, Morimoto K, Katayama Y, Matsui Y, et al. Triple combination therapy comprising osimertinib, an AXL inhibitor, and an FGFR inhibitor improves the efficacy of EGFR-mutated non-small cell lung cancer. Cancer Lett 2024;598:217124.